Automated multi-criterial treatment planning for adaptive high-dose-rate brachytherapy for locally advanced cervical cancer

Michelle Oud

A thesis presented for the degree of
Master of Science
in Biomedical Engineering

Supervisors:

dr.ir. Sebastiaan Breedveld	Erasmus University Medical Center
dr.ir. Inger-Karine Kolkman-Deurloo	Erasmus University Medical Center
dr.ir. Danny Lathouwers	Delft University of Technology
dr. Zoltán Perkó	Delft University of Technology

Delft University of Technology
July 13, 2019

Abstract

Purpose - To develop and evaluate a fast and automated multi-criterial treatment planning strategy for High-Dose-Rate (HDR) brachytherapy (BT) for patients with locally advanced cervical cancer. This automated strategy avoids suboptimal and slow manual treatment planning and results in reproducible and conformal treatment plans with a clinically favorable trade-off between multiple treatment objectives.

Methods and Materials - An automated treatment planning approach was developed using the Erasmus-iCycle framework. A wish-list containing hard constraints and prioritized objectives is required as input was configured according to the clinical protocol using 22 single-fraction training plans. Special attention was paid to establishing the clinically desired 'pear-shaped' dose distribution. To evaluate the dwell time optimization approach, 66 automatically generated single-fraction plans (PLAN_{auto}) were compared against the clinically delivered plans (PLAN_{ref}), both by blind-pairwise comparison carried out by an expert clinician and by the analysis of dosimetric plan parameters. Subsequently, for 17 complete fractioned BT treatments each consisting of 3 single-fraction BT plans, automatically generated plans (TREATMENT_{auto}) were compared against the clinically delivered plans (TREATMENT_{ref}) to evaluate dosimetric plan parameters according to the clinical protocol. The possibility of extending the algorithm with a needle selection objective was also explored on 13 test cases and its performance was evaluated by studying the number of needles selected in the optimized plans and its effect on the remaining treatment objectives.

Results - All PLAN_{auto} were considered clinically acceptable by the clinician. The clinician's plan comparison pointed strongly at an overall preference for the automated plans: in 62/66 cases the clinician preferred PLAN_{auto} over PLAN_{ref}, in three cases the overall quality was considered equal and for one case the clinical plan was preferred. For PLAN_{auto}, the mean HR-CTV $D_{90\%}$ improved while also the rectum was spared compared to PLAN_{ref}. The average optimization time was 19.5 seconds (range [4.4 – 106.4] s). The mean $D_{90\%}$ for TREATMENT_{auto} improved by + 3.0 Gy (in EQD_2) ($p<0.005$) over the whole radiotherapy treatment with differences ranging from -4.3 to +6.0 Gy, while the bladder and rectum were spared similarly ($p=0.01$, $p=0.02$ respectively). In 6/13 of the plans, the number of needles that were implanted could be reduced while still establishing sufficient plan quality.

Conclusions - Fast automated multi-criterial treatment planning for locally advanced cervical cancer HDR-BT is feasible. High-quality treatment plans are automatically generated within a clinically acceptable time frame and treatment plans have a clinically preferable trade-off between all treatment objectives. The observed improvement in dosimetric parameters, mainly the improvement of the dose to the HR-CTV, is clinically relevant. The algorithm can be extended with an approach for the optimization of the implant geometry, which could allow interactive intra-operative treatment planning.

Acknowledgements

This project was carried out under the supervision of dr.ir. Sebastiaan Breedveld, dr.ir. Inger-Karine Kolkman-Deurloo, dr.ir. Danny Lathouwers and dr. Zoltán Perkó. First of all, I would like to thank dr.ir. Sebastiaan Breedveld, who has been my daily supervisor and guided me through the project. I would like to thank dr.ir Inger-Karine Deurloo for her advise from the clinical aspect of the project, providing us with translations from clinical practice. I would like to thank my supervisors dr.ir. Danny Lathouwers and dr. Zoltán Perkó at the TU Delft for their guidance, thinking along and encouraging me to think outside of the *'Erasmus-iCycle box'*. I would also like to thank dr. Jan-Willem Mens, whose assistance has been a valuable help over the course of the project and was greatly appreciated.

Contents

1 Introduction

Cervical cancer is the fourth most common cancer in women and accounts for 7.5% of all female cancer deaths [13]. Patients diagnosed with locally advanced cervical cancer receive radiotherapy as part of their treatment. The radiotherapy treatment consists of External Beam Radiotherapy (EBRT) and high-dose-rate (HDR) brachytherapy (BT) [45]. In the external beam treatment, the patient is irradiated from the outside with X-ray beams, while in brachytherapy the patient is irradiated from the inside using a radioactive source. Including the brachytherapy within the treatment combination is shown to lead to decreased recurrence rates and increased survival [49, 19]. The radioactive source in brachytherapy is inserted within previously implanted hollow tubes. In the case of brachytherapy for cervical cancer, an applicator is implanted. The applicator consists of an intracavitary part and 10 optional interstitial plastic needles (Figure 1). The intracavitary part consists of one intra uterine tube and two ovoids. By moving the source to different positions within the applicator, different positions can be used, known as the dwell positions. The time that the radioactive source spends at a dwell position is defined as the dwell time. The dose delivered to the patient increases linearly with the dwell time.

The current clinical workflow for a single brachytherapy fraction starts with the implantation of the applicator, whereafter an MRI is acquired. Using this image, the positions of the applicator relative to the delineated structures of the patient's anatomy is defined. Treatment planning then consists of tuning the dwell times within dwell positions of the applicator.

By tuning the configuration of the implanted applicator and the dwell times, different dose distributions can be achieved. Treatment planning in brachytherapy is a complex task in which the dose distribution is optimized to tailor it specifically to the anatomy of the patient. Optimization can be performed by optimization of the applicator configuration and by the optimization of the dwell times within the implanted applicator.

The quality of the resulting dose distribution is evaluated by dose-volume based measures (in terms of the minimum dose received by the highest-receiving part of a structure) and by the shape of the isodose lines (contour lines of equal dose). The resulting optimal dose distribution is a trade-off between maximizing the dose in the target and minimizing the dose in the surrounding organs-at-risk (OARs), while the dose delivered by dwell positions from the implanted needles should be kept to a minimum and the isodose lines should be 'pear'-shaped, as shown in Figure 2 [45]. The latter makes the optimization process non-trivial compared to other treatment modalities and sites. When the resulting dose distribution complies with the clinically desired trade-off between these treatment objectives, a clinically favorable treatment plan is obtained.

Optimization of the implant geometry defines the possible dwell positions for the radioactive source. The size and position of the intracavitary applicator is fixed by the anatomy of the patient, but the number and positions of implanted interstitial needles can be tuned. The resulting implant quality is crucial for the final dose distribution and was linked to the therapy outcome [16, 48]. Optimization of the implant geometry in BT for locally advanced cervical cancer is a trade-off between the number of needles used and the resulting quality of the implant. The number of interstitial needles used should be minimized because they can cause extra trauma to the patient [16], while they are also relatively expensive. In current clinical practice, the configuration is chosen by the clinician. Mathematical op-

timization of the applicator geometry is currently uncommon, although optimization approaches have been presented [3, 16, 28, 15, 26, 22, 18], mostly for BT for prostate cancer. These approaches can not generate one optimal plan in which the number of needles used is traded-off against the quality of the treatment plan. However, these studies do show that including mathematical optimization of the implant geometry in the clinical workflow would be beneficial for the resulting dose distribution.

Optimization of the dwell times is currently still performed with a manual trial-and-error approach at institutions including the Erasmus Medical Center (MC) [16]. Dwell times are iteratively tweaked until a plan is clinically acceptable. Manual treatment planning takes around 30 minutes and with many possible active dwell positions, irregularly shaped volumes and multiple OARs, finding dwell times that would optimally satisfy the requirements by hand is a very difficult task [17]. Besides that, manually composed treatment plans are not reproducible and plan quality depends on the skills of the treatment planner and the time spent on the plan [17]. Developments in automated treatment planning for EBRT have demonstrated that it is feasible to obtain high and consistent plan quality, with automatically generated plans being largely preferred over manually generated plans [17, 18]. Automated dwell time optimization approaches for brachytherapy have mostly been presented for the treatment of prostate cancer [2, 28, 5, 43, 15, 11, 14, 25], but also for locally advanced cervical cancer [32, 17, 42]. These methods do not deliver clinically favorable trade-offs between all treatment objectives including the desired pear shape of the isodose lines, minimization of the relative dosimetric contribution by dwell positions from the interstitial needles and optimal OAR sparing.

In this work, multi-criterial optimization is performed using the Erasmus-iCycle framework to develop an automated treatment planning approach for brachytherapy for locally advanced cervical cancer. The Erasmus-iCycle system has been widely applied for many treatment sites in EBRT before [8, 50, 39, 41] and was recently extended for the optimization of brachytherapy treatment plans [7] (B-iCycle). The optimization process is guided by a wish-list, containing hard constraints and prioritized objectives. The approach is capable of automatically generating a dose distribution optimized for the prescribed target coverage and maximally spare OARs, while generating the desired shapes of the isodose lines. Also, the clinically desired trade-offs between all these objectives is obeyed and therefore the obtained dose distribution relates directly to the clinical treatment protocol. Using this approach, suboptimal and time-consuming manual treatment planning is avoided.

To automatically generate treatment plans for BT for locally advanced cervical cancer, a wish-list was designed according to the clinical protocol at the Erasmus MC using 22 representative single-fraction cases and the expertise of a clinician. To evaluate the methods, first, single-fraction plans were generated using the same treatment objectives as the clinical plans to allow straight one-to-one plan comparison. The qualitative difference between the automatically generated single-fraction plans (PLAN_{auto}) and the clinical single-fraction plans (PLAN_{ref}) was assessed in a blind study by an expert clinician. Secondly, an adaptive treatment planning protocol was designed to automatically generate adaptive treatment plans for all fractions of the BT treatment (TREATMENT_{auto}). The dosimetric effects of using automatic treatment planning was investigated by comparison of plan parameters with the clinical treatment plans for all treatment fractions (TREATMENT_{ref}). Finally, an objective to obtain the optimal configuration of the needles of the applicator was added to the wish-list to optimize both the implant configuration and the dwell times and the resulting plan quality was evaluated.

This work starts with background theory in which the clinical workflow and treatment protocol are explained (Chapter 2). In Chapter 3, a literature study into the optimization of the dose distribution for HDR brachytherapy is provided. This literature review includes approaches for the optimization of the dwell times (Chapter 3.2) and approaches for the optimization of the implant geometry (Chapter 3.3). Chapter 4 explains the proposed approach and the evaluation of the methods and in Chapter 5 the results are presented. In Chapter 6 the proposed approach and the results are discussed and in Chapter 7 concluding remarks are given.

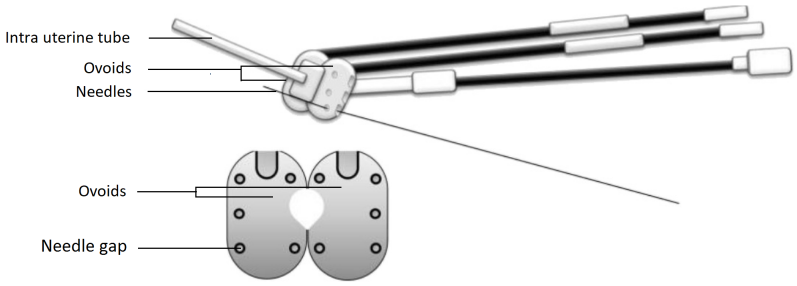

Figure 1: An applicator used in high-dose-rate brachytherapy for cervical cancer. The applicator has one intra uterine tube and two ovoids. The ovoids also serve as a template to insert a maximum number of 10 interstitial plastic needles. Image taken and modified from [19].

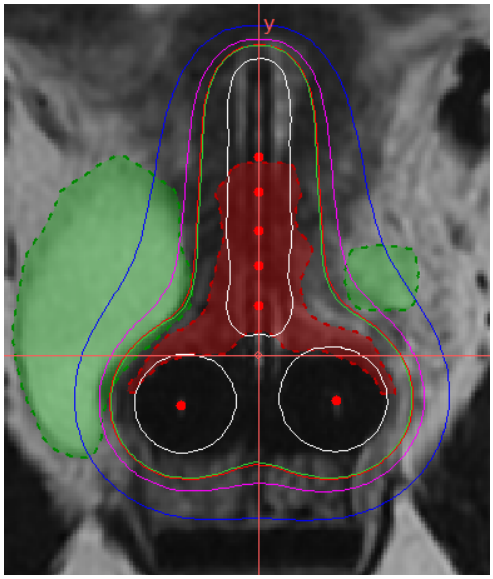

Figure 2: Typical pear-shaped dose distribution projected on 2D sagittal delineated MRI for a patient. Contours for the High-Risk Clinical Target Volume (HR-CTV) and bladder are shown in red and green respectively. Isodose lines extend beyond the HR-CTV to form the typical pear shape.

2 Clinical Background

This chapter provides general clinical background information into the treatment of locally advanced cervical cancer through high-dose-rate brachytherapy. The current clinical workflow will be described in Section 2.1 and Section 2.2 will explain the clinical treatment planning protocol in detail.

2.1 Clinical workflow

Treatment of locally advanced cervical cancer - Patients diagnosed with locally advanced cervical cancer receive radiation therapy as part of their treatment. The radiation therapy consists of external beam radiation therapy and HDR brachytherapy. An example of the radiotherapy treatment scheme is shown in Figure 3. Both EBRT and brachytherapy are divided over multiple fractions, resulting in relative sparing of the healthy tissues because healthy tissue is able to repair sub-lethal radiation damage faster compared to tumorous tissue [21]. Patients treated at the Erasmus MC receive 23 fractions of 2 Gy or 25-27 fractions of 1.8 Gy during EBRT and 3-4 fractions of BT as a boost after EBRT. The BT fractions are one week apart.

Figure 3: Example of a common radiation therapy treatment schedule for patients with locally advanced cervical cancer. Patients receive external beam radiation therapy (blue) and brachytherapy (red). Image taken and modified from [45].

Clinical workflow for a brachytherapy fraction - A schematic overview of the clinical workflow for a single brachytherapy treatment fraction is shown in Figure 4. A brachytherapy fraction starts with the implantation of the hollow tubes through which the radioactive source is led during treatment. In the case of BT for locally advanced cervical cancer, the implant is an applicator as shown in Figure 1. The applicator always has intracavitary channels, that consists of a intra uterine tube and 2 ovoids, while 0-10 optional hollow interstitial needles can also be part of the configuration. Currently at the Erasmus MC, the Utrecht applicator (Elekta AB, Stockholm, Sweden) is used. The ovoids of the applicator function as a template for the interstitial needles. Needles are essential for patients with an unfavorable anatomy, such as a relatively large target volume or a disadvantageous relation between target and OARs position [45]. The number and position of the implanted needles currently relies completely upon the insight of the clinician during the implantation phase. The clinician studies an MRI image from a prior fraction and examines the vaginal topography and tumor response [45]. Based on this, the clinician decides how many and where needles should be implanted. Figure 5 shows a schematic representation of the applicator within the patient. After the implantation of the applicator, an image of the patient is made. An MRI scan is preferred over a CT scan because it

is superior for the discrimination of the tumor tissue [34]. Using the MRI image, the location of the applicator is reconstructed on the image and relevant structures are delineated by the clinician. Using this delineated image with the reconstructed applicator, treatment planning is performed. Because for every BT fraction an MRI with fraction-specific implant geometry is obtained, each fraction can be considered an independent treatment plan. In treatment planning, the dwell times at the dwell positions within the applicator are tuned to reach a clinically favorable dose distribution. The clinical protocol for treatment planning, which describes the goals for the resulting dose distribution, will be explained in Section 2.2. To model the dose distribution, most brachytherapy treatment planning systems rely on the model established by the task group 43 (TG-43) formalism of the Association of Physicists in Medicine (AAPM) [37]. This model is outlined in Appendix A. Finally, the treatment plan is executed during which the radioactive source, usually Ir-192 in HDR-BT, is kept stationary in the dwell positions according to the treatment plan. Ir-192 decays with both β and γ emission, but only the γ radiation will reach the surrounding cells as the enclosing tube stops the β radiation [23]. The γ radiation interacts with the DNA of the cells, causing breaks in the DNA strand. Irreparable lesions in the DNA will cause cell kill.

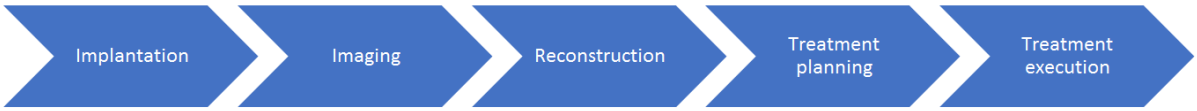

Figure 4: Schematic representation of clinical workflow.

2.2 Clinical treatment planning protocol

The aims for the dose distribution are described in the clinical protocol for treatment planning and will be explained in this section. The applicator geometry and the dwell times therein need to be tuned in order to obtain a dose distribution that complies with the clinical treatment planning protocol. A clinically desired trade-off between different treatment objectives will result in a clinically favorable dose distribution.

To evaluate the methods in this work, treatment plans for patients that were treated from 2015-2018 at the Erasmus MC were selected from the clinical database. As such, merely the clinical protocol from 2015-2018 is relevant and will be outlined in this section.

An overview of the clinical protocol for the dose distribution at the Erasmus MC from 2015-2018 is provided in Table 1. The clinical protocol consists of objectives related to the dosimetric measures of the relevant structures and objectives related to the shape of the isodose lines.

Dosimetric measures – Dosimetric measures based on the cumulative Dose Volume Histogram (DVH) (Figure 6) are a common way to evaluate the quality of the dose distribution. The cumulative DVH is a 2D representation of the 3D dose distribution, in which the fraction or volume of a structure

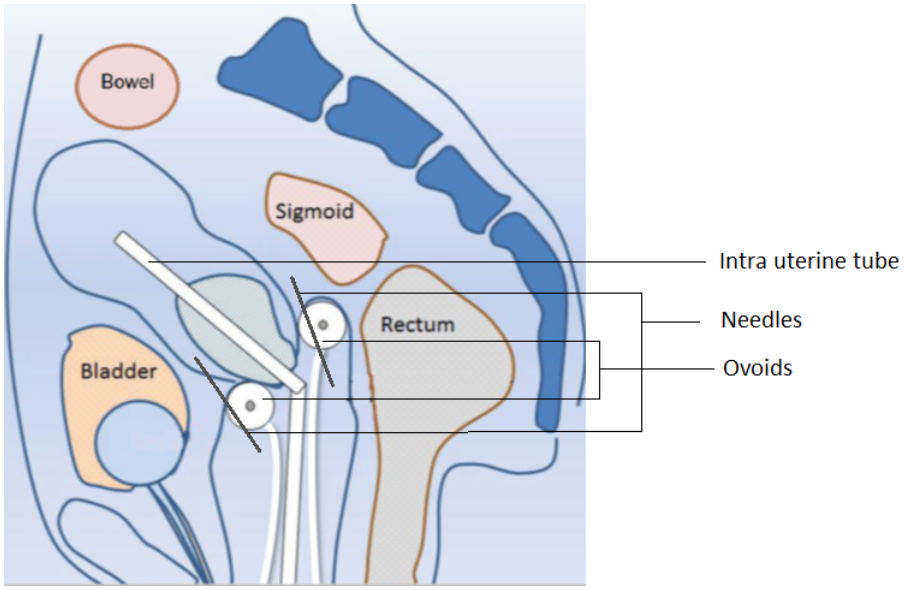

Figure 5: Schematic representation of the applicator - which consists of an intra uterine tube and two ovoids - and two extra implanted needles in the patient with the bladder, rectum, sigmoid and bowel as important organs-at-risk. Image taken and modified from [19].

that receives at least a certain dose is plotted against the dose. The minimum dose received by the highest receiving fraction or volume (x) of a structure is expressed as D_x. In the clinical treatment planning protocol, dosimetric goals and limits for the $D_{90\%}$ of the High-Risk-Clinical Target Volume (HR-CTV) and the D_{2cc} of the OARs: the bladder, rectum, sigmoid and small bowel are prescribed. The prescribed limits should always be respected, whereas a treatment plan should reach as many aims as possible. For the HR-CTV, the aim is to deliver a $D_{90\%}$ between 90 and 95 Gy. Usually, in clinical treatment planning after reaching 93.8 Gy in the HR-CTV, OAR sparing towards their goal value is preferred over increasing HR-CTV coverage. Above 95 Gy, there exists no dose-effect relationship and sparing of the OARs even below their goal value is preferred. Given the curative aim of the treatment and the relatively low average age of the patients, besides target coverage, sparing the OARs is a very important aspect of treatment planning to assure the quality of life of the patient after treatment.

Computation of full treatment dose - The clinical dosimetric protocol is only defined over the full radiotherapy treatment: as the summation of the dose over all BT and EBRT fractions in biologically equivalent doses of 2 Gy per fraction (EQD_2). Since different parts of the treatment are delivered with different fraction doses, a conversion is required to accumulate the different fractions of the treatments, therefore to compute the dose received over the full radiotherapy treatment. A common approach is to convert all physical single-fraction doses (D_{phys}) to an equivalent dose if the treatment was given in a scheme of 2 Gy per fraction, D_{EQD_2}. This is performed using the linear quadratic model according to:

$$D_{EQD_2} = D_{phys} \frac{D_{phys} + \frac{\alpha}{\beta}}{2 + \frac{\alpha}{\beta}} \tag{1}$$

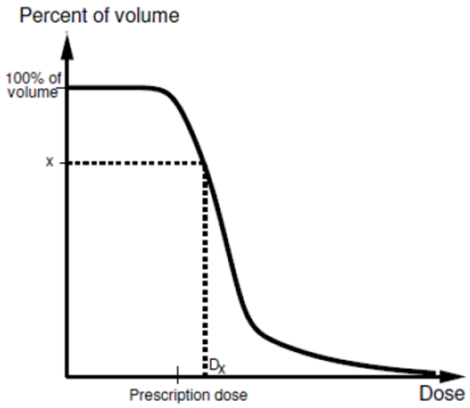

Figure 6: An example of a cumulative Dose Volume Histogram (DVH). $D_{x\%}$ is the minimum dose received by at least x% of the volume. Image taken from [23].

Here, $\frac{\alpha}{\beta}$ reflects the fractionation sensitivity of the cells, which is related to the ability of the cells to repair sub-lethal damage. The fractionation sensitivity is assumed to be 10 Gy for targets and 3 Gy for OARs and therefore the benefit in terms of equivalent dose of fractionation is larger for OARs than the disadvantage for targets. The total equivalent dose to a structure over the whole treatment is computed as the sum of the equivalent dose (D_{EQD_2}) over all EBRT and BT fractions. For the dose received during EBRT, it is assumed that the highest receiving 90% of the HR-CTV and the closest 2 cc of the OARs have received the prescribed dose. For the brachytherapy, the summation of the dosimetric values in the separate brachytherapy fraction plans can be used as a good approximation of the dosimetric parameters over the whole treatment [46], although for the different fractions the high dose region may differ significantly due to shrinkage of the tumor and changes in the implant geometry. When adding dose volume relations for the different fractions, it is assumed that the location of interest (D_{2cc} or $D_{90\%}$) is equal in all BT fractions [34].

Fraction-specific adaptive dosimetric protocol - Since the dosimetric protocol is only defined over the full EBRT+BT treatment, the different fractionation schemes during EBRT result in different dose aims and limits for the BT part of the treatment. Also, each BT fraction is geometrically unique with different dose distributions tailored to the current geometry. This results in a unique dosimetric protocol for each BT fraction, depending on the EBRT dose, the BT dose in previous fractions and the current geometry. Usually, in treatment planning at the Erasmus MC it is assumed that in every remaining BT fraction the same dose will be given to a patient as in the current fraction. However, to account for an unfavorable anatomy of the patient, the treatment planner may decide to relax the constraints in a fraction in order to reach acceptable target coverage. This should then be compensated in the remaining fractions. Over the full BT+EBRT, the limits for the OARs are always respected.

Shape of the isodose lines - Other objectives for the dose distribution are related to the shape of the isodose lines. Historically, the *pear* shape of the isodose lines is important, meaning that the dose is centered and evenly distributed in the dwell positions of the intracavitary applicator. An example of typical pear-shaped dose distribution was presented in Figure 2.

If possible, the use of the interstitial needles is limited to a minimum, with a typical dosimetric contribution from dwell positions in the needles of around 5-20%. The dose from the needles is limited to avoid hot spots in needle-adjacent areas such as connective tissue, vagina and ureters [45, 49] but also to keep the dose centered around the applicator to create the desired pear shaped isodose lines. A dose distribution with a high dosimetric contribution from the needles is shown in Figure 7.
Another objective is that there should be no hot and cold spots in the dose distribution, meaning that the dose distribution is smooth. An example of a dose distribution containing dominant dwell positions is shown in Figure 8. In brachytherapy this objective is especially important because the source is close to the target. From the source position, the dose deposition decreases spatially according to the inverse square law, which results in steep dose gradients throughout the volume. The effect is more pronounced the closer the structures are to the source. The dose inhomogeneity is an important factor in the biological effect of the treatment [34]. Cold spots in the HR-CTV might not be noticed directly from the dosimetric measurement of the $D_{90\%}$ and a smooth dose distribution is necessary to assure that the remaining 10% will also receive a reasonable dose. Besides that, having a smooth dose distribution assures that there is not an extreme high dose in one spot, reducing the chance of necrosis.

Table 1: Summary of the clinical protocol 2015-2018 at Erasmus MC. Dosimetric criteria are defined as the summation over all brachytherapy and external beam radiotherapy fractions, in which the physical dose is converted through the linear quadratic model with $\alpha/\beta = 10$ Gy for the high-risk clinical target volume (HR-CTV) and $\alpha/\beta = 3$ Gy for the organs-at-risk to a equivalent dose in 2 Gy per fraction (EQD_2). Single-fraction limits and goals are patient, organ and fraction specific.

Clinical planning protocol			
Dosimetric criteria			
Structure	**Dosimetric measure**	**Limit (EQD_2)**	**Goal (EQD_2)**
HR-CTV	$D_{90\%}$	>85 Gy	>90 <95 Gy
Bladder	D_{2cc}	<90 Gy	<80 Gy
Rectum	D_{2cc}	<75 Gy	<65 Gy
Sigmoid	D_{2cc}	<75 Gy	<70 Gy
Small Bowel	D_{2cc}	<75 Gy	<60 Gy
Other			
Soft objective	**Explanation**		
Pear shaped isodose lines	Dose centered around intracavitary applicator, evenly distributed		
Minimal needle contribution	Minimize dosimetric contribution relative to intracavitary applicator		
Smooth dose distribution	No dominant dwell positions, no cold spots		

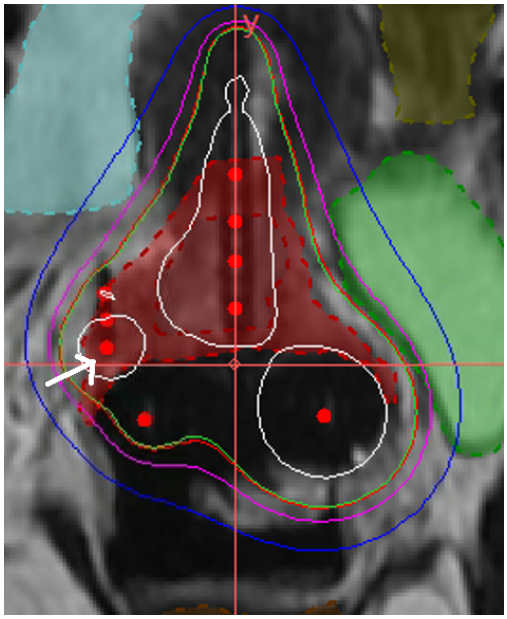

Figure 7: A slice of a dose distribution with high dosimetric contribution from dwell positions in the needles. The white arrow points at a dwell position in the needles.

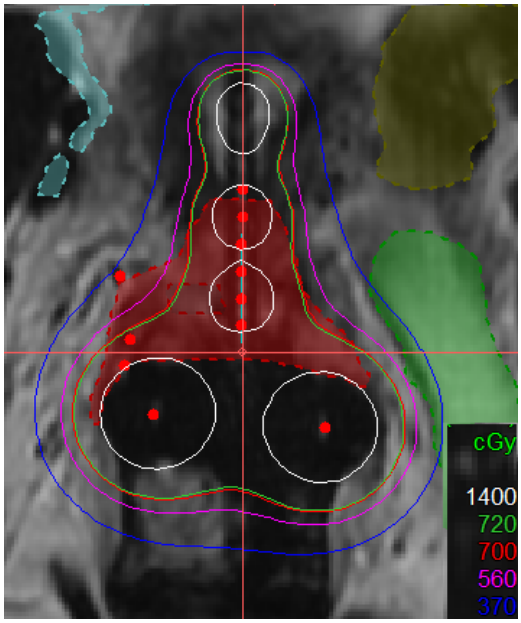

Figure 8: A slice of a dose distribution with dominant dwell positions, containing separate high dose regions. Isodose lines are not smooth.

3 Literature study

This chapter is an adapted version of Chapter 3 in my literature study: *'A literature study of Dose Optimization strategies in HDR Brachytherapy for Cervical Cancer'* and provides an overview of state-of-the-art dose optimization approaches in brachytherapy. This chapter merely describes literature until now, while in Chapter 4 the proposed approach in this work will be explained.

Structure - Optimization of the dose distribution can be performed by the optimization of the implant configuration and by the optimization of the dwell times. Section 3.1 provides the framework for this chapter, where general theory of optimization of the dose distribution in brachytherapy will be provided. In Section 3.2, dwell time optimization approaches are discussed. In Section 3.3 implant configuration optimization approaches are discussed. Section 3.4 will provide a discussion and conclusion of the literature study.

Methodology - Optimization approaches included in this literature study are approaches proposed for the optimization of brachytherapy treatment planning. In treatment planning for EBRT many advances have been made in automatic treatment planning too. Although there are many similarities between these two modalities, there are also significant differences. An example of these differences is the DVHs that look substantially different because of the steeper dose fall-off in brachytherapy. Therefore, optimization approaches in the field of EBRT are excluded from this literature study. Many approaches for automatic treatment planning for HDR brachytherapy that are discussed in this literature study have been introduced and tested for prostate brachytherapy. These approaches are included in this literature study as they are also relevant for brachytherapy for locally advanced cervical cancer. The largest difference between these two treatment sites is that in treatment planning for cervical cancer there are aims for the shape of the isodose lines. Also, there might be multiple target structures and there are more OARs involved. This results in a larger problem size and can lead to a significant increase in optimization time [17], while this also results in more complex relative priorities of the different treatment objectives. In prostate brachytherapy catheters are implanted instead of the applicator in the treatment of locally advanced cervical cancer. In prostate brachytherapy, catheters can be implanted freely and the number and the positions of the catheters should be optimized. In locally advanced cervical cancer, the intracavitary channels of the applicator are always implanted at a fixed position, given the patient anatomy. In total, 0-10 extra interstitial needles can be implanted and their positions are fixed to the positions of the ovoids of the applicator. The number and positions of these interstitial needles should be optimized in the case of locally advanced cervical cancer.

3.1 Framework

The start of the optimization process is a contoured image with the candidate dwell positions. Optimization consists of 3 steps: first, the problem is discretized by generating dose optimization points in each volume. These points represent the whole structure and the dose in these points will be optimized assuming that if the dose in these points is optimal, the dose in the entire structure is optimal. Because of the steep dose gradients in brachytherapy, relatively many dose calculation points have to be used compared to EBRT and the distribution of these points is important [23]. While in EBRT it is common to use the vertices of the 3D grid of the CT image, in brachytherapy most strategies adopt the technique proposed by Lahanas et al. [30] for generating the dose points: points are quasi randomly produced inside a bounding box of the structure, after which points that lie outside the structure or

within the implant are excluded. Figure 9 provides a 2D illustration of this process. The next step is to define a model that describes the problem. This is done by the definition of an objective function. The set of variables that lead to the minimum or the maximum of the objective function is the optimal solution. Constraints can also be added to the problem and the objective function can be optimized while subjecting to the constraints. The next step is to solve the model, thus to find the set of variables that minimize or maximize the objective function. The objective function is preferably convex: when solving non-convex objective functions there is a risk of finding a local minimum or maximum instead of a global optimum (Figure 10). Optimization strategies discussed in sections 3.2 and 3.3 differ in the definition of the model and in how the model is solved.

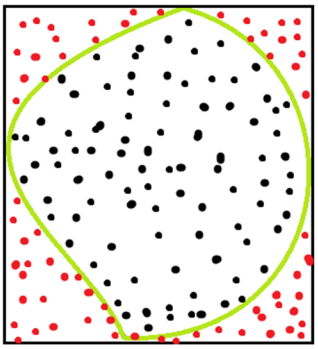

Figure 9: 2D illustration of the generation of dose optimization points for a structure (green). A bounding box is generated around a structure and dose optimization points are quasi-randomly generated within this bounding box. Points that lie outside the structure (red) are excluded.

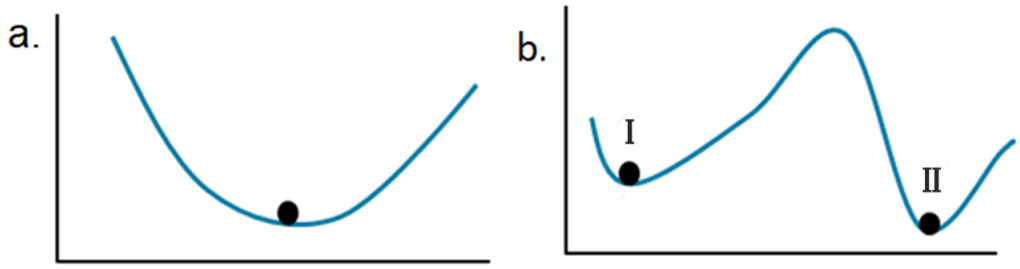

Figure 10: Illustrations of (a) A convex objective function, (b) A non-convex objective function. Optimization for a non-convex objective function could result in a solution that is a local optimum (I), not the global optimum (II).

3.2 Literature review: Dwell time optimization

All dwell time optimization strategies that will be discussed are based on manual preselection of a implant configuration during the implantation phase. The optimization approaches were divided into three categories according to their formulation of the model: approaches with a dose-based objective function, approaches with dose-volume based objective function and approaches with an alternative objective function. Unless mentioned, the approaches were designed for the treatment of prostate cancer.

3.2.1 Dose-based objective function

Formulation of the model – In a traditional inverse planning approach, a dose based objective function (DBOF) is used which works by assigning a penalty to each optimization point that has a dose outside a predefined structure-specific interval (Figure 11). The penalty is often linear in the deviation from the interval as introduced by Lessard et al. [32] and the model is then referred to as the linear penalty model. Quadratic penalty functions have also been introduced, for example by Lahanas et al. [31]. The total penalty, q, for a structure s is calculated by taking the sum of all penalties p in every optimization point, i, within a structure and averaging over all optimization points, n:

$$q_s = \sum_i \frac{p(\mathbf{x}_i)}{n_s} \tag{2}$$

In which p depends on the dwell time vector $\mathbf{x}$. The approach handles multiple objectives as the weighted sum of the penalty over all structures to one total penalty function (Q):

$$Q(x) = \sum_s w_s q_s \tag{3}$$

The weights, w, represent the relative importance of the structures and are assigned by the treatment planner. The dwell time vector x is optimized to find the minimum total penalty. In the model proposed for the treatment of locally advanced cervical cancer by Lessard et al. [32], a region around the intracavitary channels of the applicator was manually contoured to define the pear shape. The weighted sum of the dose in the HR-CTV, the pear shape and the OARs is optimized.

Solving the model - This dose-based optimization function was introduced for gynecological cancers by Lessard et al. in 2002 [32], where the solution is found using simulated annealing. Simulated annealing works by randomly stepping through the solution space, accepting a solution if it is better than the current solution and accepting it with some probability if it is worse. This probability decreases toward the end of the search process. The algorithm of Lessard et al. [32] was further developed by Alterovitz et al. [2], who formulated the optimization problem as a linear programming problem which made it possible to rapidly find the mathematical optimum of Function 3. Also, Karabis et al. [28] introduced an approach to solve the model using a quasi-newton gradient descent technique. Almost all commercially available treatment planning systems offer one of the various versions of the dose-based objective function optimization for brachytherapy treatment planning [33, 17].

Downsides and proposed solutions – The main downside of this dose-based weighted sum formulation of the model is that the dose-based penalty has poor correlation with the actual dose-volume based objectives in the clinical treatment planning protocol. Therefore, tuning the relative weights of

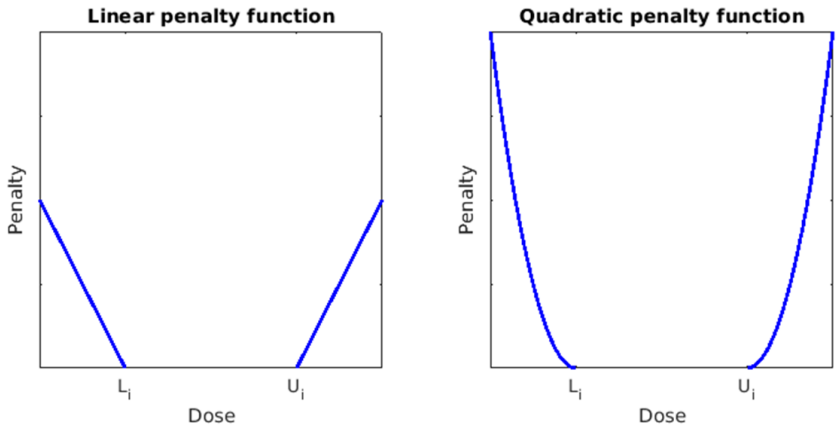

Figure 11: Penalty that is assigned to each dose optimization point in a certain structure using the linear (left) or quadratic (right) dose based penalty model. A penalty is assigned linear or quadratic in deviation from the lower bound (Li) or upper bound(Ui).

the different structures is non-intuitive in terms of the dose-volume parameters of the resulting optimal dose distribution. The algorithm has to be used in an iterative way: the treatment planner has to adjust the relative weights until a satisfactory dose distribution is reached. Finding a proper set of weights is especially difficult for gynecological treatment planning because of the multiple target areas, multiple surrounding OARs and relatively large structures [17]. Adjusting the weights is non-intuitive, time consuming and requires experience of the treatment planner.

A general patient class solution is mostly used for the initial weights, followed by iterative manual tuning of the relative weights to find an acceptable plan. However, in order for this approach to work for all patients, an automatic weight-tuning approach is strongly desired. Lahanas et al. [31] coupled the model with an evolutionary algorithm to find a certain set of weights to produce a sample of the Pareto front (NSGA-II). With the help of a decision making tool, the best plan can be chosen from the subset. Ruotsalainen et al. [40] introduced an interactive method for weight tuning. The treatment planner navigates through Pareto optimal solutions based on how he would like to see the plan change [40]. A deep-learning-trained, weight-tuning policy network was designed by Shen et al. [42]. It observes the dose-volume histograms of a plan and outputs suitable weighting factors. This approach was developed for locally advanced cervical cancer and keeps constraints on the prescribed dose in the HR-CTV and the dose in a pear shape (defined by two line segments parallel to the ovoid central axis and outer surface of the ovoids). Then, the algorithm optimizes a weighted sum for the OARs, in which the relative weights of the OARs are found using the deep-learning based approach which was trained on human decision making.

More problems relating to the dose-based penalty function problem are dominant dwell positions causing local hot spots of dose [10, 24]. Solutions for this problem are suggested in Chanjon et al. [10], who limit dwell times by introducing artificial normal tissue around the implant; in Baltas et al. [4] by restrictions on dwell time gradients and in Holm et al. [24] by introducing a piecewise linear penalty function that penalizes dose further away from the prescribed dose levels more heavily.

3.2.2 Dose-volume based objective function

Formulation of the model - Methods that can include dose-volume based parameters in the optimization model are easier to comprehend for a treatment planner as it explicitly includes the dosimetric criteria from the clinical protocol (Table 1, Chapter 2.2). Multiple research groups, such as Beliën et al. [5], Siauw et al. [43], Gorissen et al. [15], Deist and Gorissen [11] and Guthier et al. [17] have presented models that are able to optimize the dose in a target region, while subjecting to a set of dose-volume based constraints for the OARs. These constraints are hard constraints and will therefore never be violated. The optimization problem is formulated as a (mixed) integer programming problem which an objective function f is optimized under constraints in which a binary indicator c specifies for each dose optimization point i whether the accumulated dose D in this point is above or below a certain critical dose level, R. For each structure, these binary indicator variables are then summed and this sum is constrained to an organ specific fraction F of the volume [33, 43, 17]. The resulting problem is roughly of the form:

$$minimize\ f(\mathbf{x})$$

$$subject\ to:$$

$$\sum_{i \in OAR_s} c_i \leq F_s n_s\ for\ all\ OARs$$

$$c_i = \begin{cases} 1, & D_i \geq R. \\ 0, & \text{otherwise.} \end{cases}$$

Solving the model - The resulting problem is computationally expensive to solve because of the variables that are restricted to integers and no global optimum for these models can be found within a clinically acceptable time frame. To speed up computations, the proposed methods use different heuristic strategies to approximate the optimal solution, except for Gorissen et al. [15]. Gorissen et al. showed that the problem can be solved to optimality with specific solver settings within a reasonable clinical time frame [11]. However, this might be due to the low number of constraints used [25]. Beliën et al. [5] perform a simulated annealing neighborhood search to find a critical subset of voxels. Next, they impose limits on this subset by using a very steep penalty function in this area and solve the resulting problem using linear programming. Siauw et al. [43] approach the problem first by solving a model with relaxed constraints: merely constraints on the maximum dose in the OARs. Then dose optimization points in which the dose should be lower than R are defined and the problem is again optimized using these constraints. Guthier et al. [17] approximated the step function for c with a smooth logistic function (see Figure 12 in Chapter 4.3.2 for an example). This logistic function is continuously differentiable and therefore gradient descent techniques can be used to optimize the problem. The approach proposed by Guthier et al. was developed for locally advanced cervical cancer and maximizes the weighted sum of the dose in the HR-CTV and IR-CTV (a contoured region of the vagina), under the dose-volume based constraints. The desired pear shape of the isodose lines were not taken into account. Deist and Gorissen [11] approximate the optimal solution using a pure simulated annealing based approach, in which only solutions are acceptable in which all dose-volume based constraints are satisfied.

Relation with dose-based objective function - Morén et al. [33] have shown that there exists a mathematical relationship between the dose based penalty approach and the dose-volume based approach by deriving a linear penalty from the dose-volume model. They suggest that the results should be exploited to automatically calibrate the weights in the dose-based penalty functions.
,

3.2.3 Alternatives: gEUD and CVaR based objective function

As the dose-based objective function does not relate to the treatment objectives, but models that include the dose-volume based parameters are difficult to solve, two different approaches were proposed and will be discussed.

An approach by Giantsoudi et al. [14] optimizes an objective function that evaluates a measure of the generalized equivalent uniform dose (gEUD):

$$gEUD = \Big(\frac{1}{n}\sum_{i=1}^{n} D_i^a\Big)^{\frac{1}{a}} \tag{4}$$

In which a is a biological parameter accounting for the volume effect for different tissues. The gEUD incorporates the nonlinear response of targets and OARs to dose and therefore often relates better to the clinical outcome than merely dose based measures. The method optimizes the weighted sum of gEUDs of all structures using gradient descent methods. A treatment planner still needs to choose gEUD weights [25].

Holm et al. [25] created a model by approximating the dosimetric indices using a conditional value-at-risk concept (CVaR). The approach resembles constraining DVH parameters such as in the dose-volume based constraints, but instead of using the D_x (for example the D_{2cc}), which is *'the lowest dose received by the highest receiving x_{cc} of a structure'*, it uses the CVaR: *'The average dose received by the highest receiving x_{cc} of structure'*. Constraining the CVaR to a constant yields a set of linear constraints and the resulting problem can be solved more easily than the introduced mixed integer linear programming problems. Also, these linear constraints have a better correlation to the DVH-parameters from the dosimetric protocol than the weights in the dose-based penalty function. The dose to the target can be optimized under these CVaR based constraints. However, some general patient class solution for the constraints that correspond to the dosimetric limits are still necessary. With this method, instead of solving the problem approximately such as Beliën et al. [5] and Siauw et al. [43] do, Holm et al. first approximate the problem and then solve it exact.

3.3 Literature review: Optimization of the implant configuration

Treatment plan objectives – The implanted applicator always consists of an intracavitary part, with 0-10 optional interstitial needles. The goal is to place the applicator with 0-10 needles such that the resulting dose distribution is optimal. However, another objective is to use the least number of needles as possible. Although needle induced side effects are not yet studied for brachytherapy for locally advanced cervical cancer, in prostate brachytherapy implant trauma was correlated with toxicities [12] and therefore the invasive implantation of interstitial needles will likely cause extra trauma to the patients which also potentially leads to an increased risk of infection [26]. On top of that, needles are relatively expensive. As such, also for locally advanced cervical cancer it seems best to use the

minimum number of needles necessary for the treatment [16]. Guthier et al. [16] studied the number of needles selected in clinical applied plans and concluded that the number is rather large. This can be explained by the fact that more degrees of freedom will make it easier to obtain an adequate plan quality with manual planning.

Change in clinical workflow - Current implantation of applicator requires pre-selection of the needle configuration during the implantation phase based on the insight of the radiation oncologist. All implant geometry optimization approaches are based on a contoured image of the patient and therefore implementing such a implant optimization step in clinical practice would require a change in clinical workflow [16]. One option is to first carry out a pre-implantation MRI-scan and delineate relevant structures. Then, possible applicator trajectories need to be defined and digitized, with or without the use of a template. A positioning algorithm should find an optimal implant configuration and this configuration should be implanted, preferably under image guidance. Electromagnetic tracking seems a promising imaging technique to do this fast and accurately [36]. Another option is to implant the intracavitary part of the applicator first, without any interstitial needles. Then, carry out an MRI-scan, delineate structures and define the position of the applicator. Based on this, the possible needle trajectories are defined and a treatment plan, optimized for the dose distribution and the number and positions of the implanted needles, is generated. After this, needles are implanted, possibly under image guidance.

Implant geometry optimization algorithms will be discussed below and are categorized by their approach. Most optimization approaches discussed in this section were proposed for the use of prostate brachytherapy, where the implanted hollow tubes are defined as catheters. The catheter selection and positioning approaches can be used similarly to optimize the number and positions of the interstitial needles in brachytherapy for locally advanced cervical cancer.

3.3.1 Approaches based on geometry

Approaches for optimization of catheter positions proposed by Siauw et al. [44] and Poulin and Fekete [35] are purely geometric. The idea is to reach a satisfactory dose distribution by enforcing a good spatial coverage. In the Needle Planning by Integer Program (NPIP) algorithm by Siauw et al. [44], the algorithm starts with a large number of potential catheter positions and the objective is to minimize the number of catheters used while there should be a catheter within a certain radius from every point in the target volume. In the Central Voronoi Tessellations (CVT) algorithm, proposed by Poulin and Fekete [35], the only objective is to distribute a certain number of catheters as uniformly as possible in space. However, reaching the best spatial coverage does not guarantee the best dose distribution. These relatively simple approaches seem to work for the prostate but are not recommended to use for gynecological cancer because of the many relevant structures with complicated shapes.

3.3.2 Approaches with iterative catheter deletion

A heuristic approach by Ayotte et al. [3] starts by generating a plan with a large number of catheters using the linear penalty model. The catheter with the lowest fraction of total dwell time is iteratively removed whereafter a new plan is generated. The approach of Guthier et al. [18] (SACO) is similar to the approach of Ayotte et al. [3], except catheters are removed based on their contribution to the objective function instead of total amount of dwell time. The dose-based objective is to maximize the dose to the target under dose-volume based constraints according to the algorithm proposed by

Guthier et al. [16]. The catheter with the least contribution to the objective function is iteratively removed. For both algorithms the heuristic finally returns a range of different plans with a decreasing number of used catheters. The number of desired catheters in these methods should be specified, or a planner needs to choose between a series of plans with a different number of needles. The approach by Guthier et al. [16] is the only catheter optimization approach proposed for the treatment of locally advanced cervical cancer.

3.3.3 Approaches using constraints on number of catheters

Approaches using indicator constraints on the maximum number of catheters allowed were introduced by Karabis et al. [28], Gorissen et al. [15] and two algorithms by Holm et al. [26, 22]. Their model optimizes both the dwell times and dwell positions simultaneously, started by generating a high number of possible catheter positions. A binary variable b indicates whether a catheter k is used or not. Then, the sum of these variables is restricted to the maximum number of catheters N that can be used. The models are roughly of the form:

$$\begin{gathered} minimize\ f(\mathbf{x}) \\ subject\ to: \\ x_j^k \leq b_k x_{max} \\ \sum b_k \leq N \\ b_k \in \{0,1\} \end{gathered}$$

So, the model is to find a dwell time vector $\mathbf{x}$ that optimizes an objective function, while keeping constraints on the number of catheters that can be used. If a catheter k is used, b_k is equal to 1, otherwise it is 0. The constraint $x_j^k \leq b_k x_{max}$ will set the dwell time of a dwell position j in an unused catheter k to 0.

The restriction of b to an integer makes the problem computationally demanding and will lead to clinically infeasible optimization times. Therefore, the four proposed algorithms all apply methods to approach the optimal solution faster. In HIPO, Karabis et al. [28] apply simulated annealing and a scoring method to find suitable catheter positions. Using these catheter positions they optimize a weighted linear penalty function using gradient descent methods to find suitable dwell times. Unfortunately they only briefly describe their approach. Gorissen et al. [15] use a model as formulated above but also add dose-volume based constraints to the problem. The function they optimize is the dose to all dose points in the target. Specific solver settings and early termination of the optimization must speed up calculations. However, this still results in clinically infeasible computation times [16].

The model presented in Holm et al. [26] is comparable to the models by Gorissen et al. [15] and Karabis et al. [28] and aims to optimize the linear penalty model, without dose-volume constraints. They propose three different types of heuristics to solve the computationally demanding problem and conclude that the variable neighborhood search approach is superior to the other proposed approaches. This method searches for a local optimum in one neighborhood and moves to a next neighborhood if a better solution is found there. Holm et al. [22] also exploited a tailored relaxed Branch and Bound algorithm in an attempt to approach the optimal solution of the model more accurately. A Branch and Bound algorithm is an approach commonly used to solve (mixed) integer programming problems. For detailed literature about Branch and Bound methods, the reader is referred to [1]. Results showed that an optimal solution could not be found within clinically acceptable time frames.

3.3.4 Approach inspired by compressed sensing

Guthier et al. [18] (SISA) propose a compressed-sensing inspired approach to find suitable catheter positions. In their approach, the aim is to minimize the dwell times while subjecting to a constraint that bounds the maximum (linear) penalty value. However, standard compressed sensing algorithms cannot be used to solve this problem due to restrictions on the domain and the authors suggest a heuristic to solve the problem: a Splitting Inspired Subspace pursuit Algorithm (SISA). The user needs to specify the maximum number of catheters that can be used. Starting with an empty solution, subsets of dwell positions that are not yet part of the solution are iteratively added. The selection of new dwell positions is based on an estimation objective value and their dwell times and a new intermediate solution is calculated. After adding one subset of new dwell positions, the number of used catheters is evaluated. If the number of catheters of these dwell positions exceed the number of catheters that can be used, a catheter reduction step is performed. This catheter reduction step works similar to the iterative catheter deletion approach of Guthier et al. [16]: the catheters with the least contribution to the objective function are removed.

3.4 Discussion and conclusion of the literature study

Optimization of the dose distribution for cervical cancer is a complex multi-criterial problem and an automated approach that is able to trade-off the different treatment objectives is desired.

A frequently used mathematical model is a dose-based objective function, in which the weighted sum over structures is optimized. The different objectives are traded-off through their relative weights. However, the obtained penalties do not correlate with the dosimetric measures in the clinical dosimetric protocol. Therefore, there is no direct control over the relative priorities of the objectives. This switches the challenge from finding the best dwell times to finding the best weights to attribute to the structures. A well-functioning automatic-weight-tuning approach could be a valid solution to the problem. This was proposed for locally advanced cervical cancer by Shen et al. [42], however, they merely optimized the weights of the OARs under constraints on the dose in the HR-CTV, pear-shape and on the smoothness of the dose distribution.

In contrast to the weighted penalty approach, dose-volume based methods optimize the dose distribution on dose-volume based measures and therefore include the primary criteria from the treatment protocol. Due to the non-convexity of the objective function, the model is hard to solve. An option is to solve the model approximately using heuristics, or to approximate the model using another objective function such as the CVaR. These approaches do not attempt to reach as many of the treatment aims as possible, but merely focus on reaching maximal target coverage within constraints on the OARs.

For the optimization of the implant configuration, the presented approaches either require a predefined number of channels (catheters or needles), or or one needs to choose from plans with different numbers of channels. However, instead of limiting the number of channels to a maximum, an algorithm that can trade off the number of channels used to other treatment plan objectives is desired.

4 Methods and Materials

In this chapter, the proposed approach in this work is explained. Section 4.1 will describe the selected patients to train and test the proposed approach on and will explain the clinical treatment planning procedure for these patients. Section 4.2 will describe how optimization using Erasmus-iCycle works. Section 4.3 describes the configuration of the Erasmus-iCycle-based approach proposed specifically for HDR brachytherapy for locally advanced cervical cancer. Section 4.4 will explain the study setup.

4.1 Patients and clinical treatment planning

Selected patients - The patient cohort consisted of patients treated for locally advanced cervical cancer between 2015 and 2018, with stages 2.B-4.A. Patients received 23 fractions of 2 Gy or 25-27 fractions of 1.8 Gy during EBRT, followed by three or four BT fractions. During brachytherapy, patients were treated using the Utrecht applicator and 0-10 interstitial needles. For this study, 88 delivered treatment single-fraction plans for BT were selected from the clinical database of the Erasmus MC. The plans belonged to 35 different patients, while a subset of 51 plans belonged to 17 patients who received the full treatment of three BT fractions. The remaining 37 single-fraction plans belonged to 18 patients for whom one or more BT fraction of the full treatment was not selected. The reasons that one or more of these plans were not selected were either 1) a plan based on CT images instead of MRI images, making planning on DVH parameters of the target impossible, 2) missing data: images, contours or both, or 3) wrong applicator placement. For the patients who received 4 fractions of BT there was never a complete set of BT plans present, because they always received at least one CT scan.

Clinical treatment planning - Clinical treatment planning was performed for every single-fraction BT plan. Using a contoured MRI image (resolution 0.626 x 0.625 x 4 mm) with the reconstructed applicator, dwell positions were automatically generated by the Treatment Planning System (TPS) Oncentra-Brachy (version 4.5.1, Elekta AB, Stockholm, Sweden) with spacings of 5 mm. Treatment planning started from a standard plan in which all dwell positions in the intracavitary applicator were evenly active and all dwell positions in the needles were inactive. Then, the isodose lines were dragged manually by a treatment planner until a clinically favorable dose distribution was achieved. Manual planning times were not recorded, but was estimated to take around 30 minutes. These manually optimized plans were defined as the reference plans (PLAN_{ref}) in this study. For the 17 patients for whom the single-fraction plans for every BT fraction were included in the selected treatment plans, the full BT treatment plans were defined as the reference treatment (TREATMENT_{ref}) in this study. When adding up the dose (in EQD_2) received during EBRT and all BT fractions for these patients, the total dose received during the treatment was computed.

Adaptive clinical treatment planning - Since every BT fraction is geometrically unique, clinical treatment planning for the BT fraction was adaptive in which the aims and limits in the current treatment fraction depended on the dose received in previous radiotherapy fractions. As explained in Chapter 2.2, the adaptive dosimetric protocol results in a unique dosimetric protocol for each BT fraction. While the general goal is to evenly distribute the dose amongst the BT fractions, the first fractions should account for unfavorable anatomies. The clinical strategy is to accept a higher dose to the OARs in the first fractions if it is expected to be necessary to achieve a minimum HR-CTV dose in the total treatment. Over the full radiotherapy treatment, the limits for the OARs were always respected.

4.2 Automatic treatment planning with Erasmus-iCycle

Automatic treatment planning was performed in a system for automated multi-criteria treatment planning *Erasmus-iCycle*. A dose engine was implemented in Erasmus-iCycle for brachytherapy according to the TG-43 model in a different study [6]. This dose engine has been verified against the clinical dose engine of Oncentra Brachy by a gamma-analysis.

For optimization, Erasmus-iCycle requires a wish-list as input. In the wish-list, the clinical limits are defined as constraints and clinical goals as prioritized criteria. A well-tuned wish-list will result in clinically acceptable treatment plans with a clinically favorable trade-off between the treatment goals. The multi-criteria algorithm sequentially optimizes each criterion f, in order of priority, within existing constraints g:

$$minimize\, f(\mathbf{x})$$

$$subject\, to:$$

$$g(\mathbf{x}) \leq e$$

Here, $\mathbf{x}$ is a vector with variables. After each optimization, the obtained optimal solution ($\mathbf{x}^*$) for the criterion (f_n) is added as a new constraint (e_n) to the problem as:

$$g_n(\mathbf{x}) \leq e_n$$

With the constraint value for e_n:

$$e_n = \begin{cases} f_n(\mathbf{x}^*)\delta, & f_n(\mathbf{x}^*)\delta \geq G. \\ G, & f_n(\mathbf{x}^*)\delta < G. \end{cases} \tag{5}$$

Where G indicates a goal value assigned by the user. δ is a factor with which the newly added constraint is relaxed if the goal value was not reached, in order to leave room for the optimization of next criteria. After optimization of each criterion, the algorithm performs a second optimization run in which it optimizes each criterion that reached the sufficient value G in order of priority to the full extend, no stopping if G is not reached, however with stopping if a user indicated sufficient value S is reached, in order to maximally tighten the obtained results.

For each criterion, a different type of objective function can be used. Erasmus-iCycle uses a full Newton-based approach to find the optimum of the objective function, while subjecting to existing constraints. To find the step direction, the gradient and Hessian of the objective functions need to be defined. The solver of Erasmus-iCycle has functionalities to solve non-convex objective functions by encouraging convergence to a suitable optimum and avoid getting stuck in local minima [9].

4.3 Design of wish-list for BT for locally advanced cervical cancer

4.3.1 Process of wish-list design

The wish-list was configured using 22 single-fraction reference plans, selected from the 88 plans recovered from the clinical database. The 22 reference plans were selected based on the range of HR-CTV size. In close collaboration with an expert clinician at the Erasmus MC, the relative priorities among the clinical requirements for the dose distribution (Table 1, Chapter 2.2) were established and objective functions were chosen and developed. In weekly meetings, the resulting plans with the wish-list

was evaluated on the 22 single-fraction plans with the expert clinician. Based on the evaluation, the wish-list was adapted.

4.3.2 Objective functions

The wish-list contains constraints and prioritized objectives, each with their own objective function. In total, 4 different types of objective functions are used: *Quadratic, Dose-volume, Quadratic Underdose Penalty (QUP)* and *Relative*. The QUP and the relative objective functions were specifically designed and implemented for the purpose of the wish-list for BT for locally advanced cervical cancer, while also the dose-volume function required adjustments to function as an objective function in the wish-list. The quadratic objective function that was used is described in [8].

4.3.2.1 Dose-volume objective function In the dose-volume objective function, the dose D in every optimization point i is compared to a structure dependent reference dose R. The dose in a point depends on the dwell time vector $\mathbf{x}$, see Appendix A. If the objective is to minimize the dose to a volume, the penalty (c) for a dose optimization point equals:

$$c_i = \begin{cases} 0, & D_i(\mathbf{x}) < R. \\ 1, & D_i(\mathbf{x}) \geq R. \end{cases} \tag{6}$$

The sum over the penalties in all dose optimization points is taken and is averaged over the number of optimization points n. This results in a total objective function f_{dvh} for a structure:

$$f_{dvh} = \frac{1}{n} \sum_{i=1}^{n} c_i \tag{7}$$

The function is non-convex and also non-differentiable as the dose-penalty function is shaped as a step function. As such, the gradient and Hessian, required for the Newton-based optimization used in Erasmus-iCycle cannot be determined. Therefore, this approach makes use of a smooth approximation of the indicator variable c_{approx} to make the function differentiable:

$$c_{approx,i} = \frac{\frac{D_i^P}{R}}{1 + \frac{D_i^P}{R}} \tag{8}$$

Here, p is a factor that affects the steepness of the resulting sigmoid shape. The larger p, the more c_{approx} resembles c. In this implementation, $p = 100$ was used. The resulting penalty as a function of the dose is shown in Figure 12. The final objective function used in this optimization approach is:

$$f_{dvh,approx} = \frac{1}{n} \sum_{i=1}^{n} c_{approx,i} \tag{9}$$

4.3.2.2 Quadratic underdose objective function The QUP function (f_{qup}) that was implemented penalizes the negative deviation in dose D in an optimization point from a structure dependent reference dose (R) quadratically and is averaged over the number of optimization points:

$$f_{qup} = \frac{1}{n} \sum_{i=1}^{n} max(0, R - D_i)^2 \tag{10}$$

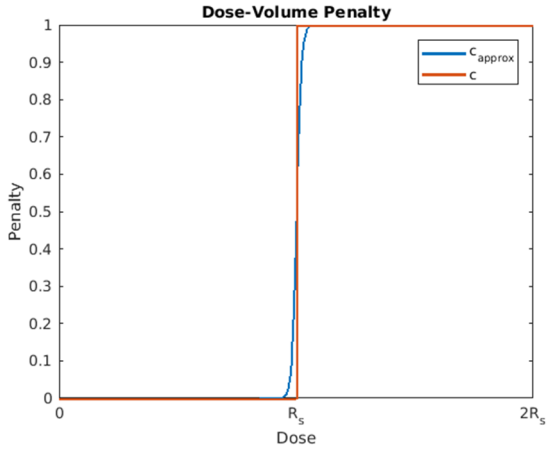

Figure 12: Dose-volume penalty for an optimization point as a function of the dose. c is a step function, in which the penalty equals 1 if the dose in a point is higher than the structure-dependent reference dose R and c is approximated by a sigmoid function c_{approx} (Equation (8)) with $p = 100$ to make the function differentiable.

Note that this function can also be used as a quadratic overdose objective function by reverting R and D_i. This function is convex, proof is provided in Appendix B1.

4.3.2.3 Relative objective function The relative objective function (f_{rel}) was specifically designed in this work to reduce the relative dosimetric contribution from dwell positions in the needles and was defined as:

$$f_{rel} = \frac{\sum \mathbf{x}_{num}}{\sum \mathbf{x}_{denom}} \tag{11}$$

Here, $\mathbf{x}_{num}$ represents a subset of the variable vector for the numerator of the fraction and $\mathbf{x}_{denom}$ is a subset of the variable vector for the denominator. The variable vector $\mathbf{x}$ is in this work a vector with the dwell times. For the purpose of minimization of the relative contribution from dwell position in the needles, $\mathbf{x}_{num}$ were the dwell times in the needles, while $\mathbf{x}_{denom}$ were all dwell times. The relative objective function is non-convex, proof is provided in Appendix B2.

4.3.3 Wish-list

General wish-list and fraction-specific limits and goals - The general wish-list is presented in Table 2. The general wish-list contains dosimetric limits and goals over the full EBRT+BT treatment. These full treatment limits and goals are converted to fraction-specific limits and goals in a fraction-specific wish-list. The computation of the parameters differs for the generation of single-fraction plans (PLAN_{auto}) and treatment plans for all BT fractions (TREATMENT_{auto}). The generation of the fraction-specific limits and goals will be explained in Section 4.3.3.1 for the generation of PLAN_{auto} and Section 4.3.3.2 for the generation of TREATMENT_{auto}.

General wish-list - The wish-list contains hard constraints on the D_{2cc} of the OARs (bladder, rectum, sigmoid and small bowel), as well as a limit on the dwell time modulation in the three channels of the intracavitary part of the applicator to enforce smoothness in the dose distribution. This smoothing constraint is enforced by limiting the difference in dwell times between adjacent dwell positions in the separate channels k to a maximum and is computed by:

$$f_{smoothing} = \sum_{k=1}^{3} \mathbf{x}_k^T M_l \mathbf{x}_k \tag{12}$$

In which l equals the length of the dwell time vector $\mathbf{x}$ in a channel and M is a l-by-l smoothing matrix. For example, if one channel consists of 5 dwell positions, for $l = 5$ this matrix looks as follows:

$$M_5 = \begin{pmatrix} 1 & -1 & 0 & 0 & 0 \\ -1 & 2 & -1 & 0 & 0 \\ 0 & -1 & 2 & -1 & 0 \\ 0 & 0 & -1 & 2 & -1 \\ 0 & 0 & 0 & 1 & -1 \end{pmatrix}$$

The maximum value allowed for $f_{smoothing}$ was empirically determined.

Within the constraints, the first priority was to establish adequate target coverage: the HR-CTV was optimized to a projected $D_{90\%}$ over the whole treatment of 90 Gy. Subsequently, the dose distribution was optimised towards a pear-shape in objectives 2-4. An artificial target structure was introduced over a 9 mm radius around all dwell positions of the intracavitary part of the applicator: the intra uterine tube and the ovoids. This is the area in which dose was delivered in clinical plans. Morphological operations (dilation and erosion) were performed on the structure to remove the sharp edges. Parts of the pear shape that overlapped with the HR-CTV and OARs were excluded. The $D_{96\%}$ of this pear structure was optimized towards the average $D_{96\%}$ in the clinical training plans. To create one homogeneous region of dose rather than risking a separation in the dose regions, a smaller pear (pear inside, with a 5 mm radius from dwell positions in the applicator) was optimized using a quadratic underdose penalty function to 12 Gy as reference dose. Figure 13 shows an example of the pear and the pear inside structure. As 4th objective, the relative contribution of the dose delivered through dwell positions in the needles was reduced using the relative objective function (Equation (11)), in which the sum of the dwell times of in dwell positions in the needles as a function of the total accumulated dwell time was minimized. The goal value was related to the number of available needles and was obtained by analyzing the trend in the clinical training plans. After establishing the correct shape of the isodose lines, as 5th priority, the goal was to further increase the HR-CTV $D_{90\%}$ towards a projected dose of 93.8 Gy, a value chosen based on the experience of the expert clinician. After that, OAR sparing was prioritized over improving target coverage: objective 6 was to reduce the D_{2cc} of all involved OARs simultaneously, however with more preference to the small bowel over the other involved OARs by assigning a weight 4 times higher than the other OARs. This weight was assigned based on the preference of the expert clinician for automatically generated training plans in which the weight of the small bowel was 4, over weights 1, 2 and 8. Finally, the dose in the HR-CTV $D_{90\%}$ was further escalated towards a projected dose to reach the desired 95 Gy.

4.3.3.1 Fraction-specific limits and goals in PLAN$_{auto}$ To enable fair single-fraction plan-to-plan comparison of the automated and clinical plans, the constraints and goals for the generation of PLAN$_{auto}$ were (partially) based on the clinical BT dose. First, for the constraints on the OARs in the plan-to-plan comparison (Cfr_{plan}), equal distribution of the dose to the OARs over all BT fractions was assumed:

$$Cfr_{eq} = \frac{limit - EBRT}{FR_{tot}} \tag{13}$$

Table 2: The general wish-list. Goals, limits and sufficient values are defined in EQD_2 as the summation of the dose over all fractions in EBRT and BT treatment, converted through the linear quadratic model with $\alpha/\beta = 10$ Gy for the high-risk clinical target volume (HR-CTV) and $\alpha/\beta = 3$ Gy for OARs in biologically equivalent doses of 2 Gy per fraction (EQD_2). The final wish-list contains fraction-specific limits and goals.

General wish-list						
Constraints						
	Volume	**Function**	**Measure**	**Limit***		
	Bladder	Dose-Volume	D_{2cc}	<90 Gy		
	Rectum	Dose-Volume	D_{2cc}	<75 Gy		
	Sigmoid	Dose-Volume	D_{2cc}	<75 Gy		
	Small Bowel	Dose-Volume	D_{2cc}	<75 Gy		
	Dwell positions applicator	Quadratic	Dwell time modulation	600		
Objectives						
Priority	**Structure**	**Function**	**Weight**	**Measure**	**Goal* (G)**	**Sufficient* (S)**
1	HR-CTV	Dose-volume	1	$D_{90\%}$	> 90 Gy	90 Gy
2	Pear	Dose-volume	1	$D_{96\%}$	> 7.9 Gy (phys)	7.9 Gy (phys)
3	Pear Inside	QUP	1		0.1	0.1
4	Needles	Relative	1	%	N**	½ N**
5	HR-CTV	Dose-volume	1	$D_{90\%}$	> 93.8 Gy	93.8 Gy
6	Bladder	Dose-volume	1	D_{2cc}	< 80 Gy	80 Gy
6	Rectum	Dose-volume	1	D_{2cc}	< 65 Gy	65 Gy
6	Sigmoid	Dose-volume	1	D_{2cc}	< 70 Gy	70 Gy
6	Small Bowel	Dose-volume	4	D_{2cc}	< 60 Gy	60 Gy
7	HR-CTV	Dose-volume	1	$D_{90\%}$	> 95 Gy	95 Gy

*The dosimetric values in Gy for limit, goal and sufficient was converted to a fraction-specific limit, goal and constraint to obtain a fraction-specific wish-list, but not for the values indicated with (phys). The limit and goal value was converted to single-fraction doses according to Equations (16) and (17) for the generation of single-fractions for PLAN$_{auto}$, and Equations (18) and (19) for the generation single-fractions of TREATMENT$_{auto}$. The sufficient value is computed similarly as the goal value.
** N = 0.1 + 0.015*(number of needles)

In which *limit* is the structure specific limit as presented in the general wish-list (Table 2), $EBRT$ represents the dose received during EBRT in EQD_2 and FR_{tot} is the total number of prescribed BT fractions. However, if clinically the constraints were relaxed in previous fractions, this should be compensated for in the current and coming fractions:

$$Cfr_{comp} = \frac{limit - EBRT - \sum BT_{clin}}{FR_{left}} \tag{14}$$

In which FR_{left} is the number of remaining BT fractions, inlcuding the current fraction and $\sum BT_{clin}$ is the sum of the dose in the previous BT fracions. The minimum of Cfr_{eq} and Cfr_{comp} was taken. However, if constraints were relaxed in the current clinical reference fraction ($PLAN_{ref}$) (due to an unfavorable anatomy of the patient), this constraint value (BT_{ref}) was also allowed in $PLAN_{auto}$:

$$Cfr_{ref} = BT_{ref} \tag{15}$$

The final limit for a specific patient and fraction in the generation of $PLAN_{auto}$ was thus equal to:

$$Cfr_{plan} = max(Cfr_{ref},\, min(Cfr_{eq}, Cfr_{comp})) \tag{16}$$

Setting the constraints this way makes it possible to fairly compare the automatically generated single-fraction $PLAN_{auto}$ to their corresponding clinical single-fraction $PLAN_{ref}$, as it guarantees to always stay below the limits unless in the current fraction clinically more dose was delivered as well. It compensates for more than average dose given in earlier fractions, however, more dose than the average dose over all fractions is not allowed unless this was clinically done as well.

For dosimetric goals for the HR-CTV and OARs, the dose in previous clinical brachytherapy fractions (BT_{clin}) was taken into account and equal distribution of the dose in the remaining fractions was assumed. The fraction-specific goal (Gfr_{plan}) was computed as:

$$Gfr_{plan} = \frac{goal - EBRT - \sum BT_{clin}}{FR_{left}} \tag{17}$$

In which *goal* is the structure specific goal as presented in the wish-list.

4.3.3.2 Fraction-specific limits and goals in $TREATMENT_{auto}$ To enable fair dosimetric comparison of the automatically generated plans and clinical plans in terms of the dosimetric protocol over the full treatment, an adaptive strategy for the fraction-specific constraints ($Cfr_{treatment}$) and goals ($Gfr_{treatment}$) was developed. The goals and constraints were based on the dose in the previous automatically generated plans for BT fractions (BT_{auto}):

$$Cfr_{treatment} = \frac{limit - EBRT - \sum BT_{auto}}{FR_{left}} \tag{18}$$

$$Gfr_{treatment} = \frac{goal - EBRT - \sum BT_{auto}}{FR_{left}} \tag{19}$$

The wish-list for the full adaptive treatment also contained two extra objectives. The first objective was to optimize the HR-CTV to the absolute minimum *goal* of 85 Gy (EQD_2), while allowing to exceed the dosimetric constraints ($Cfr_{treatment}$) on the OARs with respectively 5%, 3% and 0% in the first, second and third treatment fraction. Then, the dose in the OARs was tightened to the original constraint, before following the remainder of the main wish-list as presented in Table 2. By allowing to exceed the constraints with this 'slack' factor it was possible to deliver sufficient dose to the target in case of unfavorable anatomies in early fractions.

Appendix C provides a summary of the fraction-specific wish-list for the generation of PLAN_{auto} and TREATMENT_{auto}.

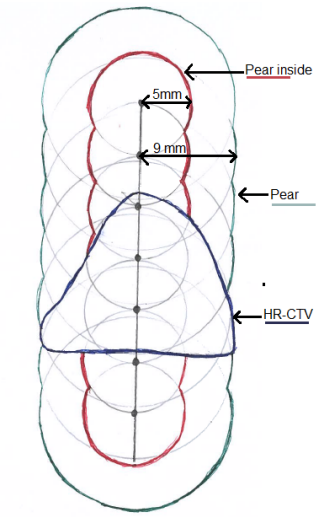

Figure 13: Schematic representation of the larger pear (green) and the smaller pear (red) with the HR-CTV (blue) and the dwell positions of the intra uterine channel of the applicator. Dwell positions in the ovoids are not shown. Pear and pear inside are artificial structures that were constructed by following the dwell positions of the intra uterine channel and ovoids of the applicator at a distance of 9 mm and 5 mm radius respectively. Parts of the pear and pear inside that overlapped with existing structures were excluded.

4.3.4 Optimization specifics

Generation of dose optimization points - In Erasmus-iCycle, the generation of dose optimization points works differently from the general approach in brachytherapy dose optimization (Chapter 3.1). Instead of the technique proposed by Lahanas et al. [30], in which the points are quasi randomly generated within a bounding box around a structure, Erasmus-iCycle generates optimization points quasi randomly on the vertices of the MRI grid with a resolution indicated by the user, as is common in optimization for EBRT. For the optimization, dose optimization points were sampled with a density of 300 voxels/cc for all involved structures.

Relaxation factor - The relaxation factor δ in Equation (5) was chosen to be 1.01, which is relatively low compared to other treatment sites. In this case the priorities of the criteria were very clear and it was not desired to leave more room for subsequent objectives if the sufficient value had not been not reached.

DVH difference – There exists a systematic difference in the computation of the DVH between Erasmus-iCycle and the clinical TPS Oncentra Brachy. An example of a DVH computed in Erasmus-iCycle in Oncentra Brachy is shown in Figure 14. This systematic difference can be attributed two things. First, the boundaries of the structures are sampled differently in the two systems. The structures in Erasmus-iCycle systematically have a larger volume than the structures in Oncentra, of which examples are listed in the table in Appendix D. Therefore, the $D_{90\%}$ of the HR-CTV computed in Erasmus-iCycle was systematically lower than the $D_{90\%}$ computed in Oncentra and the D_{2cc} of the OARs are systematically higher in Erasmus-iCycle compared to Oncentra. Another reason for the differences in DVH is the difference in the positions of the dose calculation points. In Erasmus-iCycle, the points are fixed on the 3D grid of the MRI while in Oncentra they are quasi randomly distributed over the volume. The 3D grid of the MRI especially has a low resolution in the transverse plane (4 mm). Especially if the source is close to the structure, the dose may change significantly over this distance and the dose to the structures may therefore not be representable in Erasmus-iCycle. The final DVH computations were therefore performed in Oncentra.

Region of interest optimization - To speed up the computations, only the parts of the OARs within a 35 mm radius from the dwell positions were taken into account during the optimization as beyond this distance, the maximum expected dose is much less than the constrained value. Also, since the bladder is a large structure and the region of interest is the part closest to the HR-CTV, only the 8 mm boundary was taken into account during optimization. An example of the optimization structures is shown in Figure 15. For the final DVH computation after the optimization, the full structures were used.

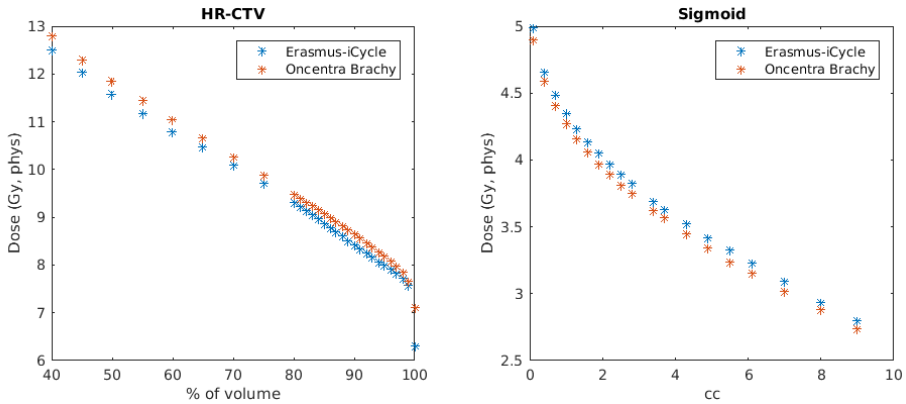

Figure 14: Dose-volume histograms of the sigmoid and HR-CTV of a patient. The size of the sigmoid was 26.6 cc in Erasmus-iCycle and 23.3 cc in Oncentra Brachy. The size of the HR-CTV was 15.2 cc in Erasmus-iCycle and 14.4 cc in Oncentra Brachy.

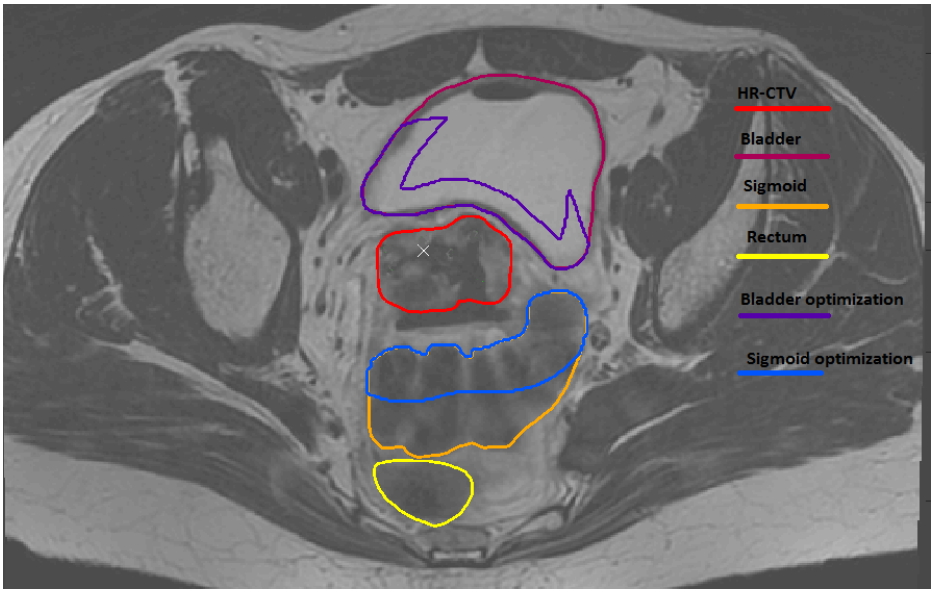

Figure 15: The optimization structures projected on a delineated MRI of a patient. To speed up computations, *Bladder optimization* and *Sigmoid optimization* were used for optimization instead of *Bladder* and *Sigmoid*. *Rectum optimization* is not shown in this slice.

4.4 Setup of studies and evaluation of the methods

The approach as explained in Section 4.3 was implemented in the Erasmus-iCycle software and treatment plans were automatically generated. Automatic treatment planning was performed on equal dwell positions and contours as the clinical plans, which were exported to Erasmus-iCycle. The air kerma strength of the radioactive source was 41325 cGy cm^2/h during all computations. The methods were evaluated in four different studies:

- Wish-list design
- Per-fraction comparison
- Per-treatment comparison
- Needle selection

4.4.1 Wish-list design

Goal - This study aimed to demonstrate the effect of the different objectives and constraints in the wish-list. The effect of the objectives and constraints on HR-CTV; Pear; Pear-inside; relative contibution of the needles; smoothing and OAR sparing on the resulting dose distribution was demonstrated by using different wish-lists, as listed in Table 3. In total, six different wish-list were used and in each consecutive wish-list another objective or constraint was added.

Selected plan - The effect of the different objectives on the dose distribution was guided by one example case, which was a patient receiving a second fraction of BT with 5 implanted needles. Table 4 shows the fraction-specific limits and goals for the example case.

Evaluation of the results - The resulting dose distributions were evaluated in terms of dosimetric parameters as listed in the clinical treatment protocol (Table 1, Chapter 2.2), and the effects were demonstrated by the comparison of slices of the dose distributions.

Table 3: The objectives and constraints in the six different wish-lists used in the demonstration of the effect of the different objectives.

	HR-CTV	OAR	Pear	Pear-inside	Smoothing	Needles	OAR
Wish-list	**Objective**	**Constraint**	**Objective**	**Objective**	**Constraint**	**Objective**	**Objective**
1	X	X					
2	X	X	X				
3	X	X	X	X			
4	X	X	X	X	X		
5	X	X	X	X	X	X	
6	X	X	X	X	X	X	X

Table 4: Fraction-specific limits and goals for an example case in the study for wish-list design.

	Measure	Cfr_{plan} (limit)	Gfr_{plan} (goal)
Bladder	D_{2cc}	7.19 Gy (phys)	6.00 Gy (phys)
Rectum	D_{2cc}	5.61 Gy (phys)	4.32 Gy (phys)
Sigmoid	D_{2cc}	5.61 Gy (phys)	5.00 Gy (phys)
Small Bowel	D_{2cc}	5.57 Gy (phys)	2.04 Gy (phys)
HR-CTV 90 Gy	$D_{90\%}$	-	9.60 Gy (phys)
HR-CTV 93.8 Gy	$D_{90\%}$	-	10.36 Gy (phys)
HR-CTV 95 Gy	$D_{90\%}$	-	10.81 Gy (phys)
Pear	$D_{96\%}$	-	7.9 Gy (phys)
Needle contribution	Relative contribution	-	13%

4.4.2 Per-fraction comparison

Goal - This study aimed to assess the qualitative difference between the automatically generated single-fraction plans ($PLAN_{auto}$) and the corresponding clinical single-fraction plan ($PLAN_{ref}$). Also, the optimization times for $PLAN_{auto}$ was studied.

Generation of $PLAN_{auto}$ - Fraction-specific wish-lists were automatically generated, in which the fraction-specific constraints and goals were computed according to Equation (16) and (17). Dwell times for the remaining 66 plans of the 88 plans from the clinical database were optimized in Erasmus-iCycle

on an Intel Core i7-7700 with 4 cores running at 3.6 GHz. The automatically generated treatment plans were exported to the clinical TPS for recomputation of the dose distribution and DVH to allow one-on-one comparison with the clinical plans, avoiding differences in the DVH computation between the two systems.

Evaluation of the results - Two approaches were used to compare PLAN_{auto} and PLAN_{ref}: first, the qualitative difference between PLAN_{auto} and PLAN_{ref} was assessed in a blind pairwise comparison for PLAN_{auto} versus the corresponding PLAN_{ref}, performed by an expert clinician. The clinician first assessed the clinical acceptability of the treatment plans and then evaluated the differences in overall, HR-CTV and OAR quality of the plans using a visual analog scale (Appendix E1). PLAN_{auto} and PLAN_{ref} were displayed side-by-side in RTStudio, a program developed at the Erasmus MC, to which the images, structures and dose distributions were exported from Oncentra Brachy. The side of the plans (left or right) was randomly chosen per case. In an extra information sheet, relevant parameters of the plans, the EBRT doses and DVH parameters of previous brachytherapy plans were provided (Appendix E2). Second, in a dosimetric analysis the $D_{90\%}$ of the HR-CTV and the D_{2cc} of the OARs were compared. Due to the varying anatomy of the patients, the results cannot be expected to be normally distributed. Therefore, statistical analysis was performed using a two sided Wilcoxon signed rank test.

4.4.3 Per-treatment comparison

Goal and selected plans- This study aimed to compare the total dose to the patients over the full BT+EBRT treatment for automatically generated plans (TREATMENT_{auto}) and the clinical reference plans (TREATMENT_{ref}) in terms of the clinical dosimetric protocol. The dosimetric parameters were studied for 17 patients who received the full treatment of three BT fractions.

Generation of $TREATMENT_{auto}$ - Wish-lists with fraction-specific constraints and goals were automatically generated for the first BT fraction, with constraints and goals computed according to Equations (18) and (19). Dwell times for the first fraction were optimized in Erasmus-iCycle. After computation of the DVH of the first fraction plans, wish-list for the second fraction were automatically generated and the second fraction was optimized. Subsequently, for the third fraction wish-list were automatically generated after computation of the DVH of the second fraction, and the third fraction was optimized in Erasmus-iCycle. The automatically generated treatment plans were exported to the clinical TPS for final computation of the dose distribution and DVH.

DVH difference -The median difference between the $D_{90\%}$ for the HR-CTV computed in Erasmus-iCycle and Oncentra Brachy was 2.5%. Because of the strict planning on the $D_{90\%}$, during optimization of the treatment plans for the per-treatment comparison, in Erasmus-iCycle this difference was taken into account by reducing the goal and sufficient value with 2.5%.

Evaluation of the results - The automatically generated treatment plans (TREATMENT_{auto}) for the full BT treatment were evaluated by comparing the dosimetric plan parameters to the clinical reference treatment (TREATMENT_{ref}) for the 17 patients. Dosimetric parameters that were evaluated were the $D_{90\%}$ of the HR-CTV and the D_{2cc} of the OARs. The total dose of the full BT+EBRT treatment was computed by summation of the single fraction doses in biologically equivalent doses of 2 Gy per fraction. Statistical analysis was again performed using two-sided Wilcoxon signed rank tests.

4.4.4 Needle selection

Goal - This study explored the possibility to extend the treatment planning approach with an objective to find the optimal needle configuration. While the intracavitary part of the applicator is always implanted, a range of 0 to 10 optional interstitial needles can be implanted. Needles are invasive and expensive, and therefore the number of implanted needles should be kept to a minimum. The aim of this study was to find clinical acceptable treatment plans with adequate target coverage and appropriate shapes of the isodose lines, while minimizing the number of needles used. If this approach works, the intracavitary part of the applicator could first be implanted and a treatment plan optimized for the number and position of the needles could be generated. The selected needles could then be implanted.

Selected plans - Needles are implanted through fixed positions in the ovoids, see Figure 1 in Chapter 1. Therefore, given the position of the intracavitary part of the applicator, it is possible to create a template for the 10 optional needle positions. However, due to restricted time of this project, no such template was created. To evaluate the potential to extend the algorithm with a needle selection objective, from the set of 88 plans from the clinical database, single-fraction plans with 7 or more implanted needles were selected, which were 13 plans in total. The number of needles used in these plans was minimized.

Methods - The optimization process consisted of 2 steps: the first step was to find out which needles could be deactivated. The second step consisted of optimization of the dose distribution according to the normal wish-list, while the dwell times in the needles that were marked to be inactive were constrained to 0.

In the first step, to find out which needles could be deactivated while still achieve a clinically acceptable treatment plan, the first part of the wish-list (Table 2) was used: Objectives 1-3 were optimized to establish adequate target coverage and the correct shape of the isodose lines. After this, a new objective was added to the wish-list: the 4th objective was to minimize the number of used needles. This was implemented as a so-called compressed sensing objective, similar to the approach presented by Jia et al. [27]. The goal was to minimize the sum of the maximum dwell time the needles, while the maximum dwell time in a needle was kept as a constraint for every needle:

$$minimize \sum_{k=1}^{N} max(\mathbf{x}_k)$$

$$subject\ to:$$

$$max(\mathbf{x}_k) \leq max(x_k^*)$$

here, $\mathbf{x}_k$ is the dwell time vector for needle k, $\mathbf{x}^*$ is the optimal dwell time vector of the previous iteration and N is the total number implanted of needles. Using this objective, the maximum dwell times in excessive needles eventually approached 0. Needles that had a total accumulated dwell time lower than 0.5 seconds were marked to be inactive.

In the second step, a new treatment plan with the same wish-list as described in Table 2 was generated with an additional constraint to set the dwell times in the needles that were marked to be inactive to 0.

To enable fair comparison with the clinically used plans, fraction-specific limits and goals were used as described in Section 4.3.3.1.

Evaluation of the results - The plans with needle reduction were defined as PLAN_{csn}. For evaluation, the number of needles used in PLAN_{csn} was compared to the number of needles used in an optimal plan, created with the same wish-list, however, without restrictions on the number of needles used. These plans are the automatically generated single-fraction plans (PLAN_{auto}). The number of needles used in these plans was also compared to the clinical treatment plans PLAN_{ref}. The effects of the needle reduction on other clinical treatment objectives was investigated as well by comparing plan parameters of PLAN_{csn} to parameters in PLAN_{auto}.

5 Results

5.1 Wish-list design

Parameters of the dose distributions that were generated with the six different wish-lists are shown in Table 5, while slices of these dose distributions are presented in Figure 16. The numbers of the different wish-list refer to the chronological evolution of the wish-list, as listed in Table 3 in Chapter 4.4.1. In wish-list 1, the most simple wish-list, the dose in the HR-CTV was optimized under dose-volume based constraints on the OARs. Although the $D_{90\%}$ of the HR-CTV is more than sufficient (goals for the dose distribution were listed in Table 4, Chapter 4.4.1), the generated dose distribution is clinically unacceptable because there is no dose in the pear, as visible in Figure 16A.

In wish-list 2, optimization of the dose in the pear-shape was added as an objective. In the resulting dose distribution, dose in the pear is sufficient as the $D_{96\%}$ is even higher than the desired 7.9 Gy, while the $D_{90\%}$ of the HR-CTV is also still more than sufficient. Because of the focus on this pear-shape, which is an area created around the intracavitary channels of the applicator, the relative dosimetric contribution of the needles also decreased from 50% to 23%. Although the dose in both the pear and HR-CTV is more than sufficient, in Figure 16A, two separate dose regions can be distinguished, rather than a single homogeneous region.

Therefore, in wish-list 3, optimization of the dose in Pear-Inside was added to the wish-list. In the result (Figure 16B), one region of dose is visible. However, when looking at the high-dose isolines of the dose distribution, there still exist separate hot-spots of dose as demonstrated in Figure 16C.

To remove these separate hot-spots of dose, a constraint on dwell time modulation was added to wish-list 4 and the effect is visible in Figure 16C. Rather than multiple hot-spots of dose, there now exists a smooth high-dose region within the HR-CTV. The smoothing objective had a neglible effect on the other parameters of the dose distribution (Table 5). However, the contribution of the relative dosimetric contibution of the needles was 35%, which is clinically undesired.

To limit the dosimetric contribution from dwell positions in the needles, the next objective was to reduce the relative contribution of the needles to at least 13% in wish-list 5. However, because all goals could be reached without any contribution from the dwell positions in the implanted needles, the needle contibution was reduced to 0% in wish-list 5.

In the resulting dose distribution, the aims for the $D_{90\%}$ of the HR-CTV and the desired shape of the isodose are reached. However, although the dosimetric limits on the OARs are not exceeded, they could be spared more towards their goal value. This was added as an objective to wish-list 6. The HR-CTV was first optimized to a physical dose of 10.36 Gy (to reach a projected dose of 93.8 Gy in EQD_2 over the total treatment), after which the next objective was to spare the OARs. If goals for the OARs would be reached, HR-CTV dose would be increased towards a projected dose of 10.81 Gy (to reach a projected dose of 95 Gy (EQD_2)). With wish-list 6, the dose in all OARs decreased compared to wish-list 5. This is also visible in Figure 16E, as the isodose lines intrude less into the bladder and sigmoid. To reach this OAR sparing, a dosimetric contribution from the needles of 12% was necessary, which is still under the goal of 13%. Since not all goals for the OARs were reached, the HR-CTV dose stayed around 10.36 Gy. Wish-list 6 was the final wish-list for the generation of $PLAN_{auto}$.

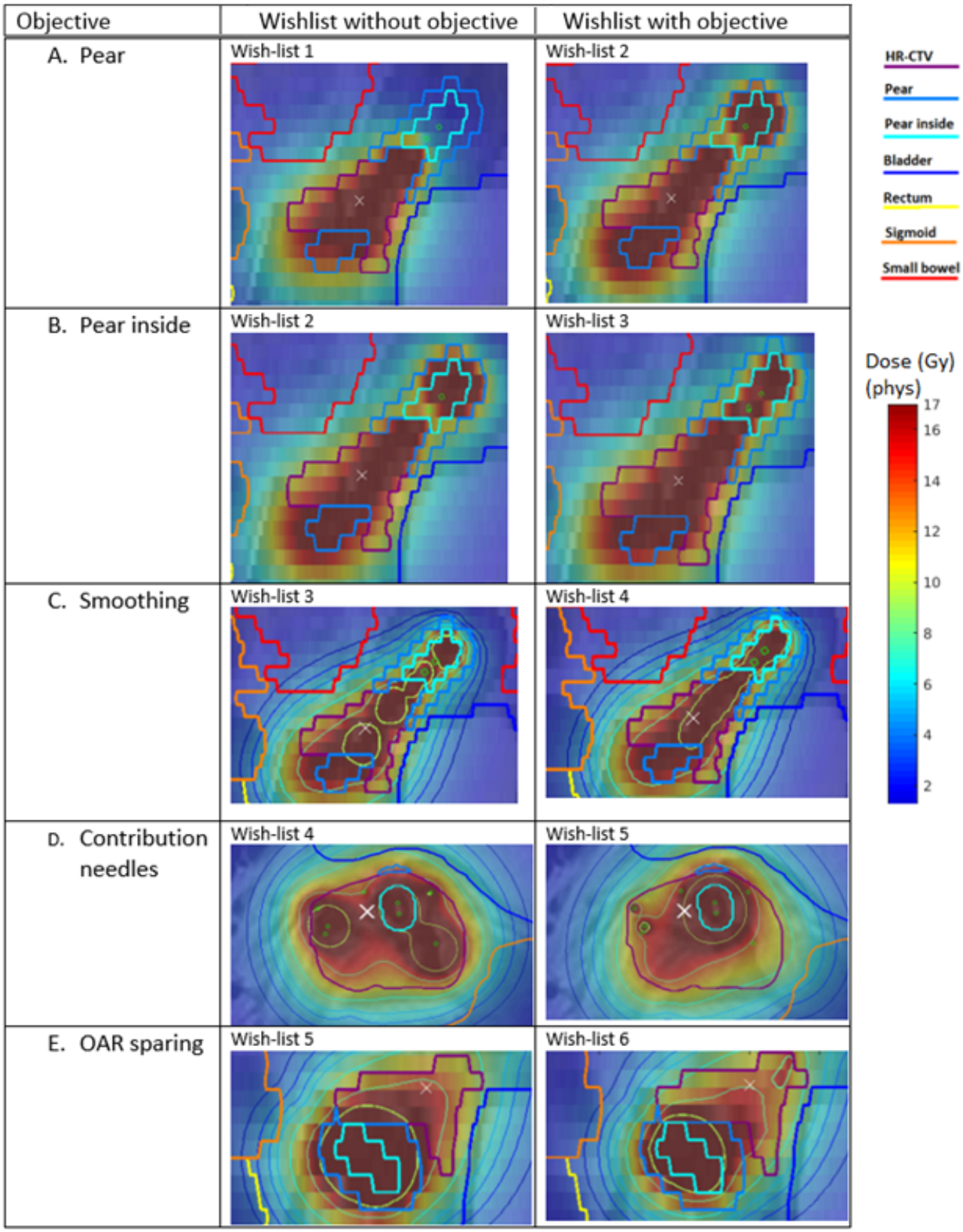

Figure 16: Slices of the dose distributions generated with six different wish-lists (1-6) for an example case. Image sets A-E show the effect of the new objective added to the wish-list. In image sets C-E, isodose lines (4,5,6,7,9,14,21 Gy) are shown.

Table 5: Parameters in the dose distribution generated with the six wish-lists for the example case.

	$D_{90\%}$ HRCTV	$D_{96\%}$ Pear	D_{2cc} Bladder	D_{2cc} Rectum	D_{2cc} Sigmoid	D_{2cc} Small bowel	Relative needle contribution	Smoothing parameter
Wish-list 1	12.38	2.1	7.18	2.70	5.60	4.74	50%	5600
Wish-list 2	11.84	9.4	7.17	3.27	5.60	4.92	23%	10100
Wish-list 3	12.25	7.9	7.18	3.01	5.60	4.84	32%	10650
Wish-list 4	12.31	7.9	7.17	3.01	5.61	4.94	35%	600
Wish-list 5	10.80	7.9	7.17	3.68	5.58	4.67	0%	600
Wish-list 6	10.32	7.9	6.63	2.77	4.76	4.04	12%	600

5.2 Per-fraction comparison

The optimization time for the 66 PLAN_{auto} was on average 19.5 s, ranging from 4.4 s to 106.4 s. Figure 17 shows a slice of an automatically generated plan on the right, with the clinical reference dose distribution on the left. The typical pear shape is visible in both plans, as the high-dose region extends beyond the HR-CTV. In the automatically generated plan, the $D_{90\%}$ of the HR-CTV was 9.44 Gy (physical dose), compared to 8.84 Gy in the clinical plan.

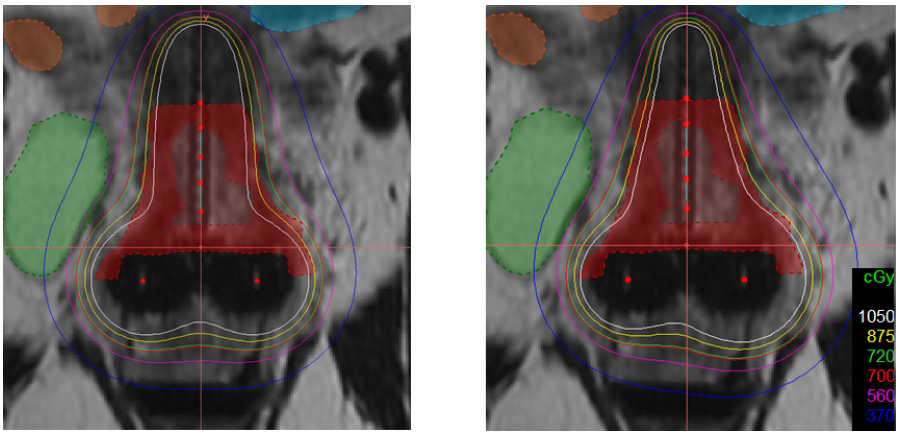

Figure 17: Sagittal slice of an MRI image with the clinical planned isodose lines of the dose distribution (left) and the isodose lines of the automatically generated dose distribution (right) projected on the contoured MRI for a patient. The high-risk clinical target volume (HR-CTV) is shown in red. The automatically generated plan shows a similar pear shape as the clinical plan.

Figure 18 shows the results of the blinded scoring by the clinician. All PLAN_{auto} were considered clinically acceptable by the clinician, while one PLAN_{ref} was not. The clinician's score reflects overall superiority for PLAN_{auto}. In 62/66 cases, overall preference was for PLAN_{auto}. In 3/66 cases, the overall quality of the plans were considered equal (score=0). In 1/66 cases, the clinical PLAN_{ref} was preferred over PLAN_{auto} in terms of overall quality. The results of the scoring on HR-CTV quality shows a similar trend as for the overall quality where in 63/66 cases PLAN_{auto} was similar or better than the clinical plan. For the OAR quality, the differences were less pronounced. Still, in 53/66

cases the PLAN_{auto} was considered similar or better and for 13/66 cases the clinical OAR quality was preferred.

Dosimetric analysis of PLAN_{auto} and PLAN_{ref} shows the same pattern as observed in the blind scoring. Boxplots for the difference in dosimetric parameters of PLAN_{auto} and PLAN_{ref} are presented in Figure 19, computed as (PLAN_{auto} - PLAN_{ref}). PLAN_{auto} showed a significant increase in HR-CTV $D_{90\%}$ compared to the PLAN_{ref} ($p<0.005$), with a mean difference in $D_{90\%}$ between PLAN_{auto} and PLAN_{ref} of +0.60 Gy (physical single-fraction dose), with differences ranging from -1.2 Gy to +2.3 Gy. In 10 plans (15%), the $D_{90\%}$ of the HR-CTV did not improve in PLAN_{auto}. However, these plans performed better on one or more of the other treatment objectives and for 8 of those cases the clinician still preferred PLAN_{auto} over PLAN_{ref} in terms of overall quality. In the remaining 2 plans, the overall quality of the plans was considered equal.

The D_{2cc} of the rectum was significantly reduced ($p<0.005$) in PLAN_{auto} compared to the PLAN_{ref} with a mean difference of -0.29 Gy (range [-1.7, +0.9] Gy). The D_{2cc} of the bladder, sigmoid and small bowel did not change significantly.

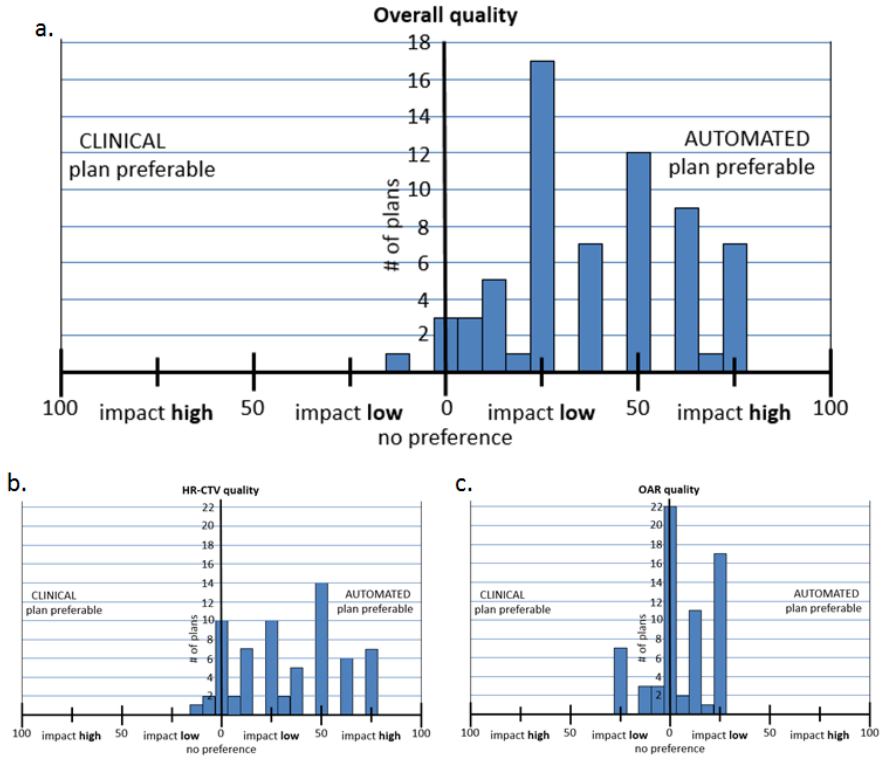

Figure 18: Histograms showing the results of the clinician's blinded side-by-side comparison of PLAN_{auto} with the clinically delivered PLAN_{ref} by visual analog scale (x-axis) for (a) overall plan quality, (b) High-Risk Clinical Target Volume (HR-CTV) quality and (c) organ-at-risk (OAR) quality for 66 plans in total.

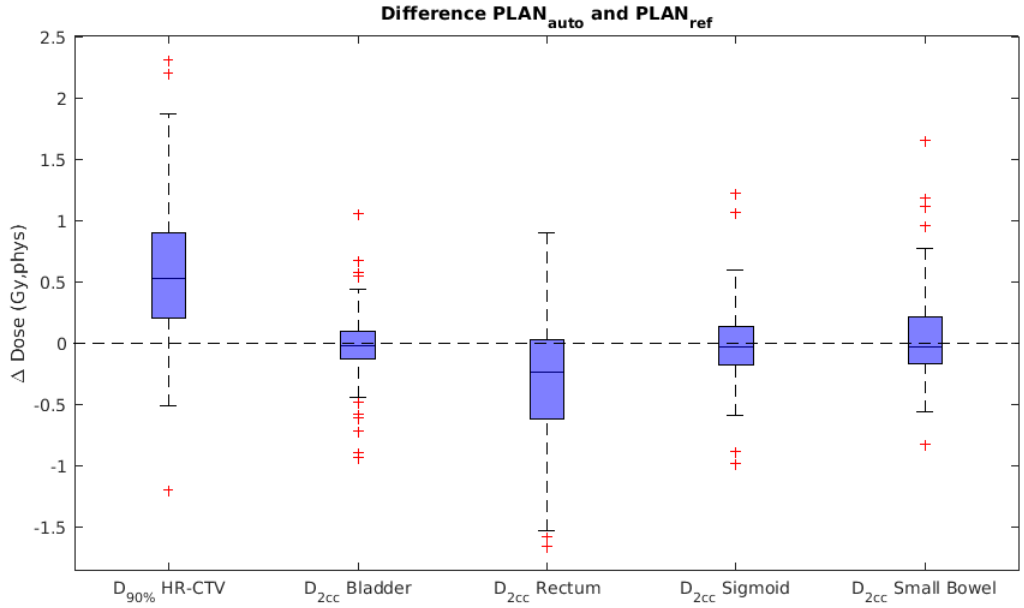

Figure 19: Boxplots showing the difference in physical single-fraction dosimetric parameters for the automatically generated plans (PLAN$_{auto}$) and the clinical reference plans (PLAN$_{ref}$) computed as (PLAN$_{auto}$ - PLAN$_{ref}$) for the D$_{90\%}$ of the High-Risk Clinical Target Volume (HR-CTV), and the D$_{2cc}$ of the organs-at-risk: bladder, rectum, sigmoid and small bowel. The central mark in the boxplot represents the median, the edges of the boxes represent the first (q_1) and third quartile (q_3). Whiskers extend to $q_3 + 1.5(q_3 - q_1)$ and $q_1 - 1.5(q_3 - q_1)$, which is the default in Matlab. Outliers are plotted individually with red + markers. Improvements in the automatically generated plan in the D$_{90\%}$ of the HR-CTV and D$_{2cc}$ of the rectum were statistically significant (Wilcoxon signed-rank test, p<0.005).

5.3 Per-treatment comparison

The D$_{90\%}$ in the HR-CTV over the full EBRT + BT treatment is shown in Figure 20 for the automatically generated plans (TREATMENT$_{auto}$) and the clinical reference plans (TREATMENT$_{ref}$). The absolute limit for the D$_{90\%}$ to the HR-CTV is 85 Gy and was always achieved in the automatic plans, whereas in two clinical reference plans (patient IDs 1 and 2) it was not. These two reference treatments therefore did not strictly comply with the requirements for clinical acceptability. This can be explained by the difficult anatomy of these patients and shows that manual treatment planning is often challenging. For patient with ID 1 it was not possible to use any needles because the sigmoid was close to the cervix, which made manual planning hard. For patient with ID 2, the clinical dose in the first fraction was extremely low, which could not be compensated for in the later fractions. In both of these cases, TREATMENT$_{auto}$ did reach a clinically acceptable target coverage, however, the goal of 90 Gy was also not reached. For patient with ID 2, the dose in the HR-CTV improved from 83.2 Gy in the clinical plan to 89.2 Gy in the automatically generated plans. Mainly in the third fraction, the automatically generated plan had an improved HR-CTV coverage. This was however achieved through a relative contribution of 46% by the needles, compared to only 23% in the clinical reference plan.

The next goal was to achieve a minimum dose of 90 Gy in the HR-CTV, in which 14/17 TREATMENT$_{auto}$ succeeded, compared to only 10/17 of TREATMENT$_{ref}$. The improvement in the D$_{90\%}$ of the HR-CTV is significant (p<0.005) and clinically relevant with a mean D$_{90\%}$ in TREATMENT$_{auto}$ of 92.9 Gy ± 1.9 Gy (EQD$_2$) compared to 89.9 Gy ± 3.7 Gy (EQD$_2$) for TREATMENT$_{ref}$. Differences ranged from -4.3 Gy to +6.0 Gy.

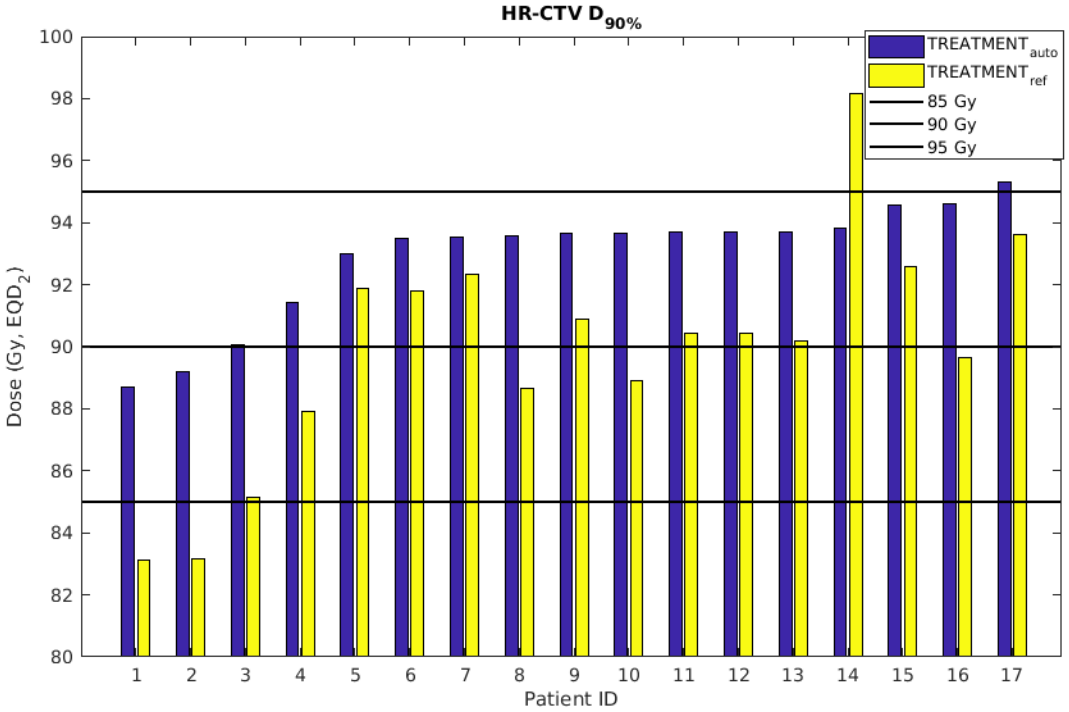

Figure 20: D$_{90\%}$ for the High-Risk Clinical Target Volume (HR-CTV) for the TREATMENT$_{auto}$ and the clinical TREATMENT$_{ref}$.

Scatter plots for the D$_{90\%}$ of the HR-CTV and the D$_{2cc}$ of the OARs are shown in Figure 21. The prescribed limit for the OARs was never exceeded, neither for TREATMENT$_{auto}$ nor for TREATMENT$_{ref}$. The dose in the bladder was significantly reduced in TREATMENT$_{auto}$ compared to TREATMENT$_{ref}$ (p=0.01) with a mean improvement of -1.1 Gy (EQD$_2$) (range [-6.6, +1.4] Gy (EQD$_2$)). The rectum was also significantly spared (p=0.02), with a mean difference of -1.9 Gy (EQD$_2$) (range [-8.7, +5.0] Gy (EQD$_2$)). There was no significant difference in the D$_{2cc}$ to the sigmoid and small bowel in the TREATMENT$_{auto}$ compared to the TREATMENT$_{ref}$ (p=0.24 and p=0.18 respectively).

In one case (patient ID 14, red diamond in Figure 21), the D$_{90\%}$ of the HR-CTV was not improved in TREATMENT$_{auto}$ compared to TREATMENT$_{ref}$. Here, the clinical D$_{90\%}$ over the full treatment was higher than 95 Gy (EQD$_2$) which is undesired if other treatment objectives, such as the goals for the OARs, are not yet reached, which were not in this case. However, the HR-CTV might have been

contoured too small in the first fraction. To make sure at least 95 Gy was delivered, the treatment planners exceeded 95 Gy in the treatment plan. In the automatically generated treatment, the $D_{90\%}$ was optimized to 93.8 Gy (EQD_2), whereafter organ sparing was prioritized. The D_{2cc} of the OARs in $TREATMENT_{auto}$ in this case were improved compared to the clinical treatment. Especially the dose to the rectum was reduced in $TREATMENT_{auto}$ (64.7 Gy (EQD_2)) compared to $TREATMENT_{ref}$ (73.4 Gy (EQD_2)).

For patient with ID 17, in $TREATMENT_{auto}$ (red pentagram in Figure 21) the dose in the HR-CTV exceeded the desired 95 Gy. However, all other objectives, such as the goals for the dosimetric goals for the OARs were reached and therefore the $D_{90\%}$ was further escalated.

5.4 Needle selection

Figure 22 shows the number of needles used in $PLAN_{csn}$ and $PLAN_{auto}$ and also shows the number of implanted needles and the number of needles used in the clinical plan ($PLAN_{ref}$). In 6/13 plans, the number of needles that was used in $PLAN_{auto}$ could be reduced in $PLAN_{csn}$, whereas this was 8/13 compared to the clinical $PLAN_{ref}$.

Reducing the number of active needles has effects on other treatment objectives, as shown in Table 6. Reducing the number of needles mainly led to a decrease in $D_{90\%}$ of the HR-CTV, while also the D_{2cc} in the OARs often increased. As expected, the relative dose contribution from dwell positions in the needles is reduced in $PLAN_{csn}$ as well.

Plan with ID 12 is an excellent example that shows the possibilities of the needle selection approach. Compared to the optimal $PLAN_{auto}$, in $PLAN_{csn}$ 3 needles were not used, while this had only a negligible effect on other treatment objectives.

In plans 6 and 7 the single-fraction $D_{90\%}$ goal for the HR-CTV of 90 Gy EQD_2 was easily reached, even without the use of needles. Therefore, none of the implanted needles were necessary for a clinically acceptable treatment plan. Reducing the number of needles here resulted mainly in a higher dose in the OARs, however, the OAR doses were still within the constraints.

In 9/13 cases, at least one of the implanted needles was not used in the clinical plan. In 7/13 cases, an implanted needle was not used in any of the plans.

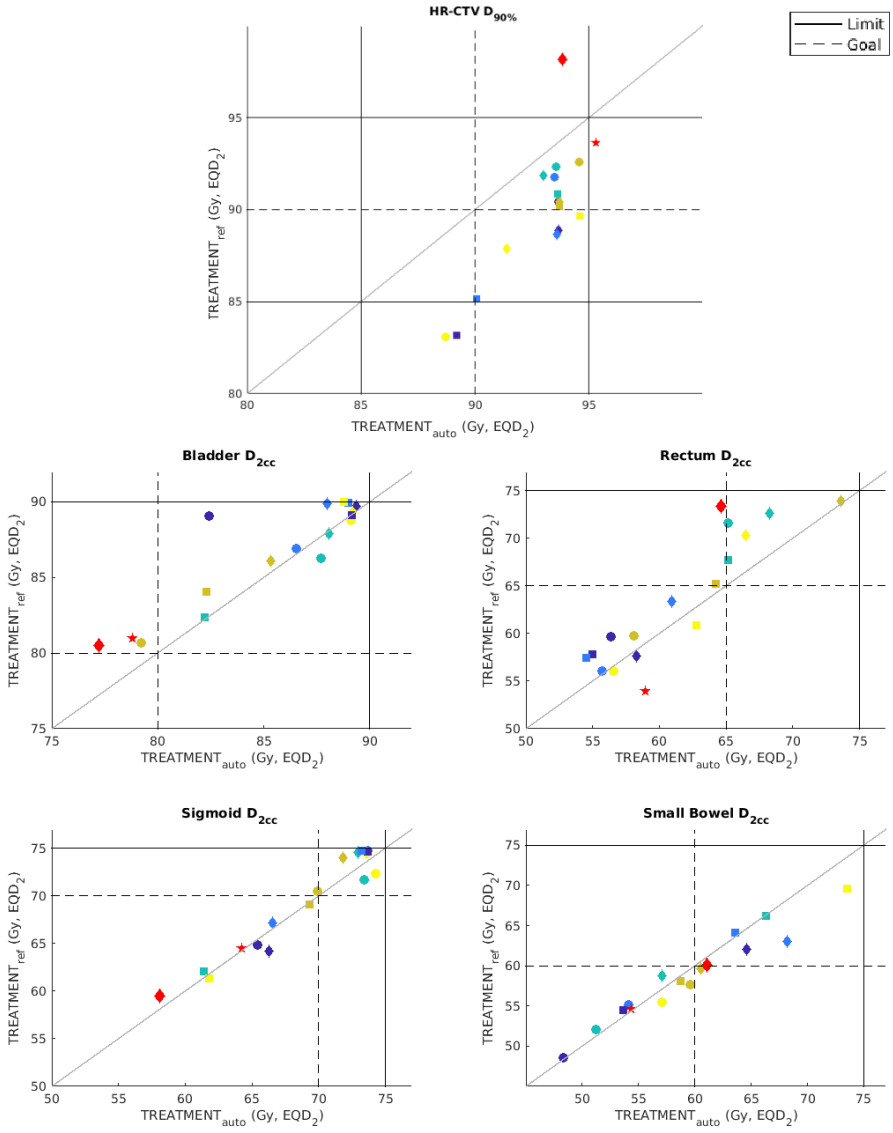

Figure 21: Scatter plots showing the $D_{90\%}$ of the High Risk-Clinical Target Volume (HR-CTV) and the D_{2cc} for the bladder, rectum sigmoid and small bowel for TREATMENT_{auto} and the clinical TREATMENT_{ref}. Every different combination of a symbol and color represents a different patient. The scatter plot for the HR-CTV shows the same data as shown in figure 20. Improvements in the $D_{90\%}$ of the HR-CTV, D_{2cc} of the bladder and rectum in TREATMENT_{auto} were statistically significant (Wilcoxon signed-rank test, $p<0.005$, $p=0.01$ and $p=0.02$ respectively). There were no significant differences for the sigmoid and small bowel.

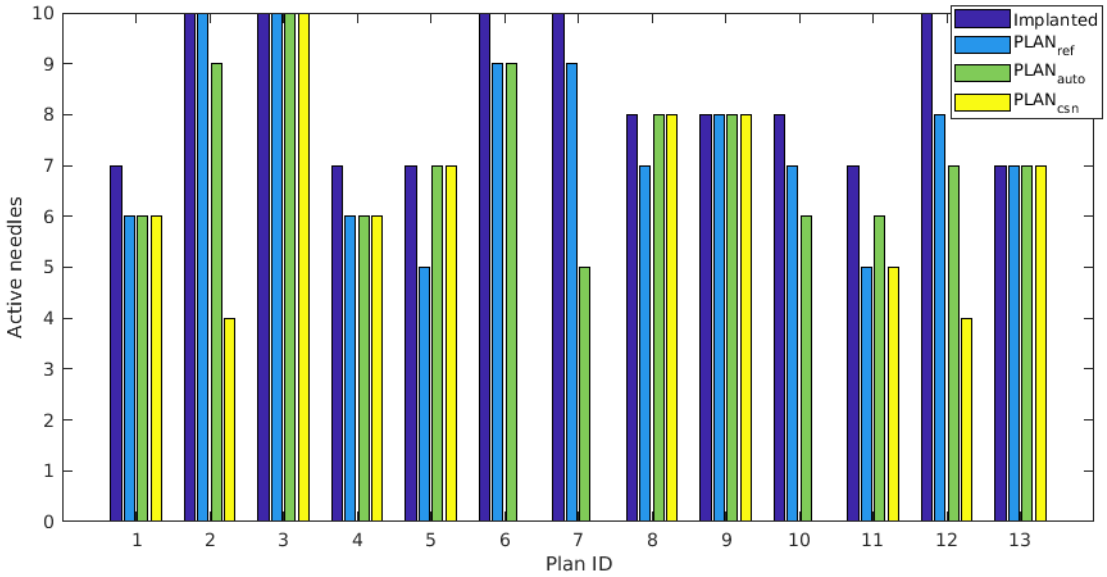

Figure 22: The number of needles implanted and used in the clinical plan (PLAN_{ref}), the plan with compressed sensing on the needles (PLAN_{csn}) and the automatically generated reference plan (PLAN_{auto}) for 13 selected cases.

Table 6: Difference in treatment objectives for the plan with needle reduction (PLAN_{csn}) and the reference plan (PLAN_{auto}) for 6 cases (single fractions) in which the number of active needles was reduced (ΔNumber used). Differences were computed as PLAN_{csn} - PLAN_{auto}, rounded to two decimals. The cells marked red indicate that the treatment objective in PLAN_{csn} became less favorable compared to the reference plan, while the cells in green indicate an improvement in the treatment objective.

	Needles	HR-CTV	Pear	Bladder	Rectum	Sigmoid	Small bowel	Relative needle contribution
Plan	**ΔNumber used**	**$\Delta D_{90\%}$ (Gy)**	**$\Delta D_{96\%}$ (Gy)**	**ΔD_{2cc} (Gy)**	**ΔD_{2cc} (Gy)**	**ΔD_{2cc} (Gy)**	**ΔD_{2cc} (Gy)**	**Δ% (Gy)**
2	-5	-0.12	0.00	0.00	-0.09	-0.01	0.15	-0.02
6	-9	0.10	0.07	0.72	0.92	0.48	0.10	-0.17
7	-5	-0.15	0.14	0.39	0.08	0.14	-0.01	-0.10
10	-6	-0.17	-0.05	0.48	0.39	0.44	0.72	-0.19
11	-1	-0.02	0.00	0.00	0.00	0.00	0.00	0.00
12	-3	-0.01	-0.04	-0.04	0.00	0.02	0.01	0.00

6 Discussion

Clinically favorable dose distribution - Optimization of the dose distribution for BT for locally advanced cervical cancer is a complex multi-criterial problem. The treatment protocol consists of dose-volume based constraints and aims, as well as aims related to the shape of the dose distribution. A treatment plan must reach as many aims as possible, while never exceed the dosimetric constraint for the OARs. An automated treatment planning approach should be able to take into account these objectives and trade-off their relative priorities in a way that complies with the clinical protocol, in order to obtain a clinically favorable dose distribution.

Wish-list – In this approach, the Erasmus-iCycle framework was used to automatically generate treatment plans. Erasmus-iCycle requires the input of a wish-list to guide the optimization process. The manual design of the treatment site specific wish-list is an essential part of the optimization process. The manual tweaking of the different parameters in the wish-list is a time consuming process. Many input parameters in the wish-list required to be tuned: the objectives need to be modelled in the form of an objective function and their respective goal values need to be chosen. Also, the relative priorities of the objectives need to be established. Extra artificial structures were used to create the right shape of the isodose lines. In this case, the choices for the parameters in the wish-list were often derived from the 22 clinical training plans and based on the preference of the clinician, but were tuned to based on empirical information. The obtained configuration of the wish-list is a general class solution for the 22 training plans. For individual treatment plans, another configuration might result in a better treatment plan. In the future, creating a suitable wish-list should become less time consuming, with automatically optimized parameters [20].

DVH objective - The non-convex dose-volume based objective functions were a crucial part of the wish-list. They were not only used as constraints for the dose to the OAR, but also as an objective to optimize the dose in the target and OARs. They were essential to rank the relative importance of the objectives, such as the trade-off between the optimization of the dose in the target versus sparing of the OARs. Using convex linear dose-based objective functions or LTCP objective functions yielded bad correlation with the actual dose-volume to the structures and resulted in a lack of intuitive control over the dose distribution. The bad correlation between the convex alternatives and the dose-volume parameters of the resulting dose distribution has been reported before [25]. The dose-volume based objective functions were therefore used, with an approximation of the step function to make the function differentiable. Due to the non-convexity of this function, the problem becomes harder to solve.

Change wish-list according to protocol – The current wish-list was designed for the treatment protocol at the Erasmus MC for the time in which the patient cohort was treated (2015-2018). The wish-list can and should be adapted to changes in the protocol. There exists large variation in treatment aims for the dose distribution among different institutions [47]. The Embrace II protocol, written by a committee of the GEC ESTRO network [45], contains guidelines to clarify and unify treatment objectives. The Erasmus MC recently started to comply with this protocol, making the current wish-list (unfortunately) unusable in clinical practice. The new protocol contains additions to the old protocol, for example goals for the $D_{98\%}$ of the Gross Tumor Volume (GTV) and Intermediate-Risk – CTV (IR-CTV), as well as a goal for the dose in the recto-vaginal and vaginal-lateral dose points (contoured by a clinician). If the IR-CTV is contoured, the artificial pear-shape becomes less relevant. Because the new protocol contains more objectives, clinical treatment planning times have increased significantly

and manually trading-off all objectives has become even more complex. Therefore, this automated approach, when adapted to the Embrace II protocol, is even more valuable.

Per-fraction comparison - To allow a fair one-by-one comparison between PLAN_{auto} and PLAN_{ref}, to constraints on the OARs in the automatically generated plans had to be adapted to the constraints in the clinical treatment plans, while also the dose in the previous clinical brachytherapy fractions had to be taken into account.
The qualitative plan-by-plan evaluation in which PLAN_{auto} was compared to PLAN_{ref} shows it is possible to automatically generate clinically acceptable plans of higher quality than the corresponding clinical plans. The blind scoring pointed at overall superiority for PLAN_{auto}. Although in 10 cases the HR-CTV dose in PLAN_{auto} was lower compared to PLAN_{ref}, the clinician considered the overall plan quality equal or better in each of those plans. This indicates that the trade-off between the multiple objectives is clinically preferable. It also indicates that approaches that mainly focus on maximizing target coverage, such as presented by [5, 43, 17, 15, 11], are not sufficient.
In theory, the clinician's scoring might include some bias. The clinical protocol leaves some grey areas, in which the relative priorities of the objectives are undefined which leaves room for the personal interpretation of the treating clinician. In the wish-list and therefore in the automatically generated plans, the relative priorities were tailored to the interpretation of one clinician, who also performed the blind comparison. Part of the selected clinical plans consisted of patients treated by this clinician, while another part did not. Therefore, a subset of clinical plans may have had different relative priorities of the objectives.

Per-treatment comparison - Adaptive treatment plans for all three BT fractions were automatically generated in the per-treatment comparison. To allow compensation for an unfavorable anatomy of the patient, a 'slack' factor was introduced, in which the constraints on the OARs could be exceeded in order to reach sufficient target coverage in the first and second fraction. In the dosimetric study, automatically generated treatment plans (TREATMENT_{auto}) were compared to their clinically used counterpart (TREATMENT_{ref}). Results show that the automatically generated treatment plans have an improved HR-CTV coverage, as well as a reduced dose to the rectum and bladder. The dosimetric differences are more meaningful in this study compared to the per-fraction comparison because the dosimetric measures directly relate to the treatment protocol and therefore provide direct insight in the impact of the treatment. Also, during the generation of the treatment plans in TREATMENT_{auto}, clinical delivered doses were not taken into account, as opposed to PLAN_{auto}. Therefore, it resembles a real clinical situation.

Needle selection - The needle selection study shows the potential of adding optimization of the applicator configuration to the approach for the optimization of the dose distribution. However, steps need to be taken to implement the approach. First, a template for the needle positions should be created and verified to predict needle positions from the inserted intracavitary part of the applicator. Then, fine tuning of the approach is necessary, as the clinically favorable trade-off between the treatment objectives should be established. The relative priorities were currently not tuned to the clinical protocol, leading to clinically undesired trade-offs between the number of needles used and dosimetric parameters, such as in cases 6 and 10, for which the reduction of the number of needles used results in a much higher dose in the OARs. After the relative priorities are established, the approach should also be made robust against implantation errors, which occur frequently because of bending and deflection of the needles. If implemented, a fast dwell position optimization approach combined with

a fast dwell time optimization approach would allow interactive intra-operative treatment planning. Ideally, in the nearby future needles are positioned under image guidance based on an individualized and automatically generated plan that is optimized for the number and positions of needles and dwell times, either robust to implantation errors or fast enough to allow on-line adaptive treatment planning.

Optimization times - With an average optimization time below 20 seconds, the dwell time optimization approach is fast enough to be used in clinical practice, leading to a huge speed-up compared to manual treatment planning which takes around 30 minutes. However, to allow interactive, intra-operative treatment planning in which the treatment plans are optimized for the applicator configuration as well as the dwell times during the implantation phase, optimization times of several seconds are desired and the optimization time should be decreased.

The proposed approach compared to other approaches - The proposed approach in this work is superior to this and other published approaches in terms of the ability to optimize multiple criteria. The dose-volume based approach for dwell time optimization is most similar to the approach proposed by Guthier et al. [17], however the presented approach includes extra objectives. Besides the optimization of the dose to the target under dose-volume based constraints, such as proposed in [5, 43, 15, 17, 11], this approach is able to obtain the prescribed target coverage, maximally spare the OARs while generating the desired shape of the isodose lines and obeying clinically desired trade-offs between all these objectives.
When optimizing the dose in the OARs, optimization of the dose in the small bowel was prioritized over the other OARs by assigning a weight 4 times as high to this structure in the approach proposed in this work. However, this weight may not always be clinically preferable because this depends on the DVHs of the structures. This optimization step could be extended with the automatic weight tuning approach proposed by Shen et al. [42], in which the relative weights of the OARs are automatically tuned according to the DVHs of the structures in order to obtain a clinically more preferable dose distribution. However, the optimization times of 4-5 of this approach is currently too slow to use in clinical practice.
For the optimization of the needle configuration, this approach generates a single treatment plan, in which the number of needles used are traded-off against other treatment objectives. Other approaches either generate multiple plans with different subsets of needle configurations, or require a predined number of channels. The compressed sensing idea behind this approach is most similar to the approach presented in Guthier et al. [18], however they could not optimize the dwell time vector directly and required a heuristic approach to solve their model.

DVH disagreement – Systematic disagreements between DVH computation of Erasmus-iCycle and the clinical TPS Oncentra disturbed the optimization on the relative priorities of the exact DVHs, as the $D_{90\%}$ of the HR-CTV was systematically lower in Erasmus-iCycle compared to Oncentra while the D_{2cc} of the OARs were systematically higher. Due to these differences, the obtained results are suboptimal in some cases and the trade-off between HR-CTV coverage, pear shape, use of the needles and OAR sparing is different than modelled. The DVH difference was especially inconvenient in the generation of TREATMENT_{auto}, because the dose in three fractions was added, enlarging the differences. Therefore the median difference in dose was used to compensate during the optimization of TREATMENT_{auto}. Despite the differences, results indicate that auto-planning is clinically acceptable and the trade-offs are sufficient. However, the results can be improved by improving DVH agreement between the clinical TPS Oncentra and Erasmus-iCycle. Although a gamma analysis has already been

performed, it should be performed again to verify whether it was correct. Besides that, the edges of the structures as well as the optimization points should be sampled similarly in both systems.

7 Conclusion

In this work, a fully automated multi-criterial approach for BT treatment planning for locally advanced cervical cancer was presented. Using the Erasmus-iCycle framework, first, the dwell times of the radioactive source in fixed dwell positions were optimized.

The required wish-list was designed and tailored to the treatment protocol at the Erasmus MC. A quadratic underdose and a relative objective function were implemented in the Erasmus-iCycle software for the purpose of this wish-list. The wish-list contains hard constraints on dosimetric indices of the OARs and on the dwell time modulation of dwell positions in the applicator to enforce a smooth dose distribution. The wish-list contains objectives to maximize the dose in the HR-CTV and to minimize the dose in the OARs. To generate the desired shape of the isodose lines, objectives to optimize the dose in artificial pear shapes and an objective to reduce the relative dosimetric contribution from dwell positions within the needles were implemented.

In the automatic generation of the full BT treatment plans, adaptive treatment planning was performed by taking into account the dose in previous BT and EBRT fractions, while also, in case of an unfavorable anatomy, allowing to exceed single-fraction constraints in early fractions in order to reach a minimum dose in the target. Over the whole radiation treatment, the clinical constraints were always respected.

Treatment plans were generated within a clinically acceptable time frame, with an average optimization time of 19.5 seconds. The resulting quality of the automatically generated treatment plans was higher than the manual treatment plans, which was both confirmed in a blind side-by-side comparison of single-fraction treatment plans and by a dosimetric evaluation over the whole radiation treatment. In the resulting dose distributions, a clinically preferable trade-off between the treatment objectives was obtained.

This work shows that fast automated multi-criterial treatment planning for locally advanced cervical cancer HDR-BT is feasible. Unfortunately, the presented approach can not be used in clinical practice because of a recent change in the clinical protocol. However, a new wish-list can be created according to the new universal clinical protocol.

The quality of the resulting treatment plans can be improved by improving DVH agreement between Erasmus-iCycle and the clinical TPS, therefore obtaining the trade-off between the objectives exactly as modelled.

The proposed approach is unique from other presented approaches for taking into account multiple criteria, including maximally sparing the OARs, obtaining the desired pear shape of the dose distribution and minimizing the dosimetric contribution from the needles. Also, none of the other automated approaches presented an adaptive treatment planning protocol, taking into account dose received in previous radiotherapy treatments and unfavorable anatomies.

To optimize the possible dwell positions as well as the dwell times, this work also shows the potential of extending the algorithm with a needle selection approach, in which the number of needles implanted can be traded-off against the quality of the resulting dose distribution. This is unique com-

pared to other proposed approaches for the optimization of the implant geometry, in which the number of implanted channels is either predefined or multiple plans with different configurations are generated.

Before performing any further studies, first, the computation of the DVHs in Erasmus-iCycle and Oncentra should coincide. In a future study, a wish-list should be tailored to the new universal clinical protocol (Embrace II) and automatically generated treatment plans should be compared to manually composed plans in a prospective study. The evaluation should be performed both in a blind plan-by-plan study, preferably performed by multiple clinicians from different institutions, as well as in a dosimetric analysis. A implant configuration optimization approach, robust for deviations in needle implantation, should be implemented and evaluated. To allow interactive intra-operative treatment planning, needles should be implanted under image-guidance and optimization times should be no longer than several seconds.

Appendix

Appendix A - TG-43 model

To compute the dose delivered by the radioactive source to the patient, most brachytherapy treatment planning systems rely on the model established by Task Group 43 (TG-43) of the Association of Physicists in Medicine (AAPM) [37]. The model relies on many approximations and assumptions. For example, the formalism assumes that the attenuation and absorbed dose in all tissue types is equal to attenuation and absorbed dose in water. Also, ignores shielding by the applicator and applicator radiation interactions are ignored [38].
The dose rate $\dot{D}$ in water at a distance (r, θ) from a single source can be modelled according to the TG-43 using the following equation [37]:

$$\dot{D}(r,\theta) = S_k \Lambda \frac{G_L(r,\theta)}{G_L(r_0,\theta_0)} g_L(r) F(r,\theta) \tag{20}$$

Here, S_k equals the air-kerma strength of the source ($cGycm^2h^{-1}$), Λ equals the dose rate constant in water (cm^{-1}). Multiplying these two will give the dose rate in water at a reference point. The geometry function ($\frac{G_L(r,\theta)}{G(r_0,\theta_0)}$) is measured relative to a reference point at with $r_0 = 1\,cm$ and $\theta_0 = 90°$. It takes into account the spatial distribution of the activity within the source: how line-like or point-like the source is. In the case of a point source, it approaches r^{-2}. The radial dose function g_L accounts for scattering and attenuation along the transverse axis caused by the interaction of the photons with the medium and source materials. $F(r,\theta)$ is the anisotropy function and accounts for the variation in the dose off the transverse plane. [37, 29, 38]

The accumulated dose D in a point i as a result of the contribution of the dwell positions j can be calculated by the multiplication of the dose rate with their dwell times (x) and summation over all dwell positions:

$$D_i = \sum_j \dot{D}_{ij} x_j \tag{21}$$

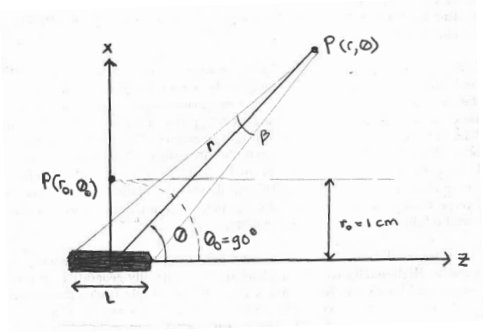

Figure 23: Illustration of the coordinate system used for brachytherapy dosimetry calculations according to the TG-43 model. Image copied and adapted from [37].

Appendix B - Convexity of the objective functions

For optimization purposes, it is desired to know whether a function is convex because when optimizing a convex function, a local optimum is the global optimum, while non-convex functions contain local optima that are not the global optimum, as was illustrated in Figure 10, Chapter 3.1. In this section, the convexity of the quadratic underdose and the relative objective function is defined.

Definition *A function* $f\colon \mathbb{R}^n \to \mathbb{R}$ *is convex if for all* x, y *in its domain and for all* $0 \leq t \leq 1$*, the following condition holds:*

$$f(tx + (1-t)y) \leq tf(x) + (1-t)f(y) \tag{22}$$

Graphically, this means that if this condition is satisfied, for each pair of points on the graph of f, $(x, f(x))$ and $(y, f(y))$, the line segment connecting the points is never located beneath the graph of f. Therefore an optimum is the global optimum, as demonstrated in Figure 24.

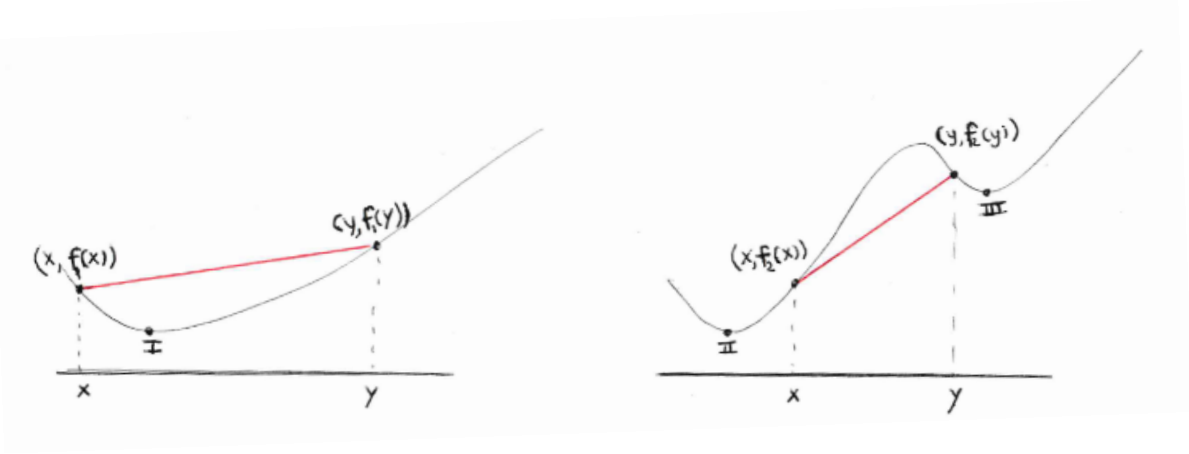

Figure 24: Illustration of the definition of a convex function. On the left, a convex function with the line segment connecting two points on f_1 located above the graph with one minimum, I. On the right a non-convex function, with a line segment connecting two points on f_2 located under the graph. Here, II is the global minimum while III is a local minimum.

Appendix B1 - Quadratic Underdose Objective function

Proof will be provided that the quadratic underdose penalty is convex. The quadratic underdose penalty, f_{qup}, defined is as:

$$f_{qup} = \frac{1}{n}\sum_{i=1}^{n} max(0, R - D_i)^2 \tag{23}$$

Substitution of f_{qup} in the convexity condition as defined in Equation (22) gives:

$$max(0, (R - (tx + (1-t)y)))^2) \leq t\, max(0, (R-x))^2 + (1-t)\, max(0, (R-y))^2 \qquad t \in [0,1] \tag{24}$$

Because of the *max* operator in this function, 4 different scenarios can be distinguished:

- Scenario A: $R - x \leq 0,\ R - y \leq 0$
- Scenario B: $R - x \leq 0,\ R - y > 0$
- Scenario C: $R - x > 0,\ R - y > 0$
- Scenario D: $R - x > 0,\ R - y \leq 0$

In each of these scenarios, x and y can be expressed as a function of R, using non-negative constants a and b:

- Scenario A: $x = R + a, y = R + b$
- Scenario B: $x = R + a, y = R - b$
- Scenario C: $x = R - a, y = R - b$
- Scenario D: $x = R - a, y = R + b$

By substitution of each of these Scenarios in Equation (24), it can be proven that for each case, the convexity condition is always satisfied.

Scenario A Substitution of scenario A in Equation (24) gives:

$$\begin{aligned} max(0, (R - (t(R+a) + (1-t)(R+b))))^2 \leq \\ t\, max(0, (R - (R+a)))^2 + (1-t)\, max(0, (R - (R+b)))^2 \\ t \in [0,1],\ a \geq 0,\ b \geq 0 \end{aligned} \tag{25}$$

Simplifying gives:

$$\begin{aligned} max(0, -ta + b(t-1))^2 \leq 0 \\ with\ t \in [0,1],\ a \geq 0,\ b \geq 0 \end{aligned} \tag{26}$$

Since $-ta + b(t-1)$ is always negative, this condition always holds.

Scenario B Substitution of Scenario B in Equation (24) gives:

$$\begin{aligned} max(0, (R - (t(R+a) + (1-t)(R-b))))^2 \leq \\ t\, max(0, (R - (R+a)))^2 + (1-t)\, max(0, (R - (R-b)))^2 \\ with\ t \in [0,1],\ a \geq 0,\ b \geq 0 \end{aligned} \tag{27}$$

Simplifying gives:

$$max(0, -ta + b - tb)^2 \leq (1-t)b^2 \tag{28}$$

Here, two new scenarios can be distinguished:

- Scenario B1: $-ta + b - tb \leq 0$

- Scenario B2: $-ta + b - tb > 0$

For Scenario B1:

$$\begin{aligned} 0 &\leq (1-t)b^2 \\ with\, t &\in [0,1],\ a \geq 0,\ b \geq 0 \end{aligned} \tag{29}$$

Which is always valid. For Scenario B2:

$$\begin{aligned} (-ta + b - tb)^2 &\leq (1-t)b^2 \\ with\ \ -ta - b + tb &> 0 \\ with\, t &\in [0,1],\ a \geq 0,\ b \geq 0 \end{aligned} \tag{30}$$

Taking the square root on both sides and reformulation gives:

$$\begin{aligned} -ta + b(1-t) &\leq b\sqrt{(1-t)} \\ with\ \ -ta - b + tb &> 0 \\ with\, t &\in [0,1],\ a \geq 0,\ b \geq 0 \end{aligned} \tag{31}$$

Because $-ta$ is always negative and $1 - t \leq 1$, the following always applies:

$$-ta + b(1-t) \leq -ta + b\sqrt{1-t} \leq b\sqrt{1-t} \tag{32}$$

And therefore this condition is always satisfied.

Scenario C Substitution of Scenario C in Equation (24) gives:

$$\begin{aligned} max(0, (R - (t(R-a) + (1-t)(R-b))))^2 \leq \\ t\, max(0, (R - (R-a)))^2 + (1-t)\, max(0, (R - (R-b)))^2 \\ with\, t \in [0,1],\ a \geq 0,\ b \geq 0 \end{aligned} \tag{33}$$

The equation can be simplifyied in the following steps:

$$max(0, ta + b - tb)^2 \leq ta^2 + (1-t)b^2 \tag{34}$$

$$(ta + b - tb)^2 \leq ta^2 + (1-t)b^2 \tag{35}$$

$$\begin{aligned} t(a-b)^2 - (a+b)^2 &\leq 0 \\ with\, t &\in [0,1],\ a \geq 0,\ b \geq 0 \end{aligned} \tag{36}$$

Since $a + b$ is always larger than $a - b$, the condition is always satisfied.

Scenario D Substitution of Scenario D in Equation (24) gives:

$$\begin{aligned} max(0, (R - (t(R-a) + (1-t)(R+b))))^2 \leq \\ tmax(0, (R - (R-a)))^2 + (1-t)\, max(0, (R - (R+b)))^2 \\ with\, t \in [0,1],\ a \geq 0,\ b \geq 0 \end{aligned} \tag{37}$$

Simplifying gives:

$$\begin{aligned} max(0, ta - b + tb)^2 \leq ta^2 \\ with\, t \in [0,1],\ a \geq 0,\ b \geq 0 \end{aligned} \tag{38}$$

Here, two scenario's can be distinguished:

- Scenario D1: $ta - b + tb \leq 0$
- Scenario D2: $ta - b + tb > 0$

For Scenario D1, Equation (38) becomes:

$$\begin{aligned} 0 \leq ta^2 \\ with\, t \in [0,1],\ a > 0 \end{aligned} \tag{39}$$

This scenario is always valid. In case of Scenario D2, a should always be larger than $\frac{-b(t-1)}{t}$. Writing out the brackets of Equation (38) gives:

$$\begin{aligned} t^2a^2 - 2tab + 2t^2ab + b^2 - tb^2 + t^2b^2 \leq ta^2 \\ with\, t \in [0,1],\ a > \frac{-b(t-1)}{t},\ b > 0 \end{aligned} \tag{40}$$

Simplifying and rewriting this equation gives:

$$\begin{aligned} a^2(t-1)t + b(at(2t-2)) + b^2((t-2)(t+1)) \leq 0 \\ with\, t \in [0,1],\ a > \frac{-b(t-1)}{b},\ b > 0 \end{aligned} \tag{41}$$

Since $(t-1), (2t-2)$ and $(t-2)$ are always negative, while the other parts of the equation are always positive, the condition is always satisfied.

For all scenarios, the convexity condition is satisfied and therefore the quadratic underdose objective function is convex.

Appendix B2 - Relative Objective function

The relative objective function f_{rel} is non-convex, which will be proven by contradiction. In the most simple form of the relative objective function, the relative objective function can be defined as

$$f_{rel} = \frac{x_1}{x_2} \tag{42}$$

Substituting of f_{rel} into the convexity condition (Equation (22)) gives:

$$\begin{aligned} \frac{tx_1 + (1-t)y_1}{tx_2 + (1-t)y_2} \leq t\frac{x_1}{x_2} + (1-t)\frac{y_1}{y_2} \\ t \in [0,1] \end{aligned} \tag{43}$$

Let $x_1 = 1$, $x_2 = 2$, $y_1 = 3$, $y_2 = 4$ and $t = 0.01$. Then it follows that the condition is not satisfied. Therefore, this function is non-convex.

Appendix C - Fraction-specific wish-list

The fraction-specific wish-list is shown in Figure 25.

Fraction-specific wish-list

Constraints

	Structure	Measure	Fr1 Single-fraction	Fr1 Total treatment	Fr2 Single-fraction	Fr2 Total treatment	Fr3 Single-fraction	Fr3 Total treatment
	Bladder	D_{2cc}	$< \frac{90-EBRT}{3^*}$ **	$< \frac{90-EBRT}{3} \cdot 1.05$	$< \frac{90-EBRT}{3^*}$ ***	$< \frac{90-EBRT-BTauto_1}{2} \cdot 1.03$	$< \frac{90-EBRT}{3^*}$ ***	$< \frac{90-EBRT-BTauto_1-BTauto_2}{1}$
	Rectum	D_{2cc}	$< \frac{75-EBRT}{3^*}$ **	$< \frac{75-EBRT}{3} \cdot 1.05$	$< \frac{75-EBRT}{3^*}$ ***	$< \frac{75-EBRT-BTauto_1}{2} \cdot 1.03$	$< \frac{75-EBRT}{3^*}$ ***	$< \frac{75-EBRT-BTauto_1-BTauto_2}{1}$
	Sigmoid	D_{2cc}	$< \frac{75-EBRT}{3^*}$ **	$< \frac{75-EBRT}{3} \cdot 1.05$	$< \frac{75-EBRT}{3^*}$ ***	$< \frac{75-EBRT-BTauto_1}{2} \cdot 1.03$	$< \frac{75-EBRT}{3^*}$ ***	$< \frac{75-EBRT-BTauto_1-BTauto_2}{1}$
	Small bowel	D_{2cc}	$< \frac{75-EBRT}{3^*}$ **	$< \frac{75-EBRT}{3} \cdot 1.05$	$< \frac{75-EBRT}{3^*}$ ***	$< \frac{75-EBRT-BTauto_1}{2} \cdot 1.03$	$< \frac{75-EBRT}{3^*}$ ***	$< \frac{75-EBRT-BTauto_1-BTauto_2}{1}$
	Dwell pos. applicator	Smooth	600	600	600	600	600	600

Objectives

Priority SF	Priority TT	Structure	Measure	Fr1 Single-fraction	Fr1 Total treatment	Fr2 Single-fraction	Fr2 Total treatment	Fr3 Single-fraction	Fr3 Total treatment
-	1	HR-CTV	$D_{90\%}$	-	$> \frac{85-EBRT}{3}$	-	$> \frac{85-EBRT-BTauto_1}{2}$		-
-	2	Bladder	D_{2cc}	-	$< \frac{90-EBRT}{3}$	-	$< \frac{90-EBRT-BTauto_1}{2}$	-	-
-	2	Sigmoid	D_{2cc}	-	$< \frac{75-EBRT}{3}$	-	$< \frac{75-EBRT-BTauto_1}{2}$	-	-
-	2	Rectum	D_{2cc}	-	$< \frac{75-EBRT}{3}$	-	$< \frac{75-EBRT-BTauto_1}{2}$	-	-
-	2	Small bowel	D_{2cc}	-	$< \frac{75-EBRT}{3}$	-	$< \frac{75-EBRT-BTauto_1}{2}$	-	-
1	3	HR-CTV	$D_{90\%}$	$> \frac{90-EBRT}{3^*}$	$> \frac{90-EBRT}{3}$	$> \frac{90-EBRT-BTclin_1}{2^*}$	$> \frac{90-EBRT-BTauto_1}{2}$	$> \frac{90-EBRT-BTclin_1-BTclin_2}{1^*}$	$> \frac{90-EBRT-BTauto_1-BTauto_2}{1}$
2	4	Pear	$D_{360\%}$	7.9 Gy (phys)	7.9 Gy (phys)	7.9 Gy (phys)	7.9 Gy (phys)	7.9 Gy (phys)	7.9 Gy (phys)
3	5	Pear-inside	QUP	0.1, 12 Gy (phys)	0.1, 12 Gy (phys)	0.1, 12 Gy (phys)	0.1, 12 Gy (phys)	0.1, 12 Gy (phys)	0.1, 12 Gy (phys)
4	6	Needles	Relative	0.1 + 0.015 · #needles	0.1 + 0.015 · #needles	0.1 + 0.015 · #needles	0.1 + 0.015 · #needles	0.1 + 0.015 · #needles	0.1 + 0.015 · #needles
5	7	HR-CTV	$D_{90\%}$	$> \frac{93.8-EBRT}{3^*}$	$> \frac{93.8-EBRT}{3}$	$> \frac{93.8-EBRT-BTclin_1}{2^*}$	$> \frac{93.8-EBRT-BTauto_1}{2}$	$> \frac{93.8-EBRT-BTclin_1-BTclin_2}{1^*}$	$> \frac{93.8-EBRT-BTauto_1-BTauto_2}{1}$
6	8	Bladder	D_{2cc}	$< \frac{80-EBRT}{3^*}$	$< \frac{80-EBRT}{3}$	$< \frac{80-EBRT-BTclin_1}{2^*}$	$< \frac{80-EBRT-BTauto_1}{2}$	$< \frac{80-EBRT-BTclin_1-BTclin_2}{1}$	$< \frac{80-EBRT-BTauto_1-BTauto_2}{1}$
6	8	Rectum	D_{2cc}	$< \frac{65-EBRT}{3^*}$	$< \frac{65-EBRT}{3}$	$< \frac{65-EBRT-BTclin_1}{2^*}$	$< \frac{65-EBRT-BTauto_1}{2}$	$< \frac{65-EBRT-BTclin_1-BTclin_2}{1}$	$< \frac{65-EBRT-BTauto_1-BTauto_2}{1}$
6	8	Sigmoid	D_{2cc}	$< \frac{70-EBRT}{3^*}$	$< \frac{70-EBRT}{3}$	$< \frac{70-EBRT-BTclin_1}{2^*}$	$< \frac{70-EBRT-BTauto_1}{2}$	$< \frac{70-EBRT-BTclin_1-BTclin_2}{1}$	$< \frac{70-EBRT-BTauto_1-BTauto_2}{1}$
6	8	Small bowel	D_{2cc}	$< \frac{60-EBRT}{3^*}$	$< \frac{60-EBRT}{3}$	$< \frac{60-EBRT-BTclin_1}{2^*}$	$< \frac{60-EBRT-BTauto_1}{2}$	$< \frac{60-EBRT-BTclin_1-BTclin_2}{1}$	$< \frac{60-EBRT-BTauto_1-BTauto_2}{1}$
7	9	HR-CTV	$D_{90\%}$	$> \frac{95-EBRT}{3^*}$	$> \frac{95-EBRT}{3}$	$> \frac{95-EBRT-BTclin_1}{2^*}$	$> \frac{95-EBRT-BTauto_1}{2}$	$> \frac{95-EBRT-BTclin_1-BTclin_2}{1^*}$	$> \frac{95-EBRT-BTauto_1-BTauto_2}{1}$

Figure 25: The fraction-specific wish-list. Values for the constraints and objectives differ per objective per fraction (Fr1, Fr2 and Fr3) and are different in case of the generation of a single-fraction (SF) plan ($PLAN_{auto}$) and the generation of the total treatment (TT) plans ($TREATMENT_{auto}$). They depend on the dose received during EBRT and on the dose in previous BT fraction, either in the previous clinically given plan BTclin, or on the previous automatically generated plan BTauto.

* In case of 3 BT fractions, otherwise +1

** Unless clinically higher

*** Unless dose in previous BT fraction(s) higher, unless clinically higher.

Appendix D

PatID	System	HR-CTV (cc)	Bladder (cc)	Rectum (cc)	Sigmoid (cc)	Small bowel (cc)
Pat1fr1	iCycle	92,1	156	80,2	51,4	14,4
	Oncentra	89,9	152,9	74,8	44,1	13,6
Pat8fr2	iCycle	19,6	236,5	44,3	56,3	98,9
	Oncentra	18,9	234,4	43,2	51,4	94,5
Pat31fr2	iCycle	23,3	187,6	9,4	103,6	123,4
	Oncentra	22,8	185,1	10,3	95,4	116,6
Pat47fr1	iCycle	49	253,3	86,7	78,6	4,9
	Oncentra	48,1	250,2	83,9	73,9	4,2

Table 7: The volume of structures for four random test cases computed in Erasmus-iCycle and the clinical treatment planning system Oncentra Brachy.

Appendix E - Blind scoring of PLAN_{auto} and PLAN_{ref}

Appendix E1 - Scoring form

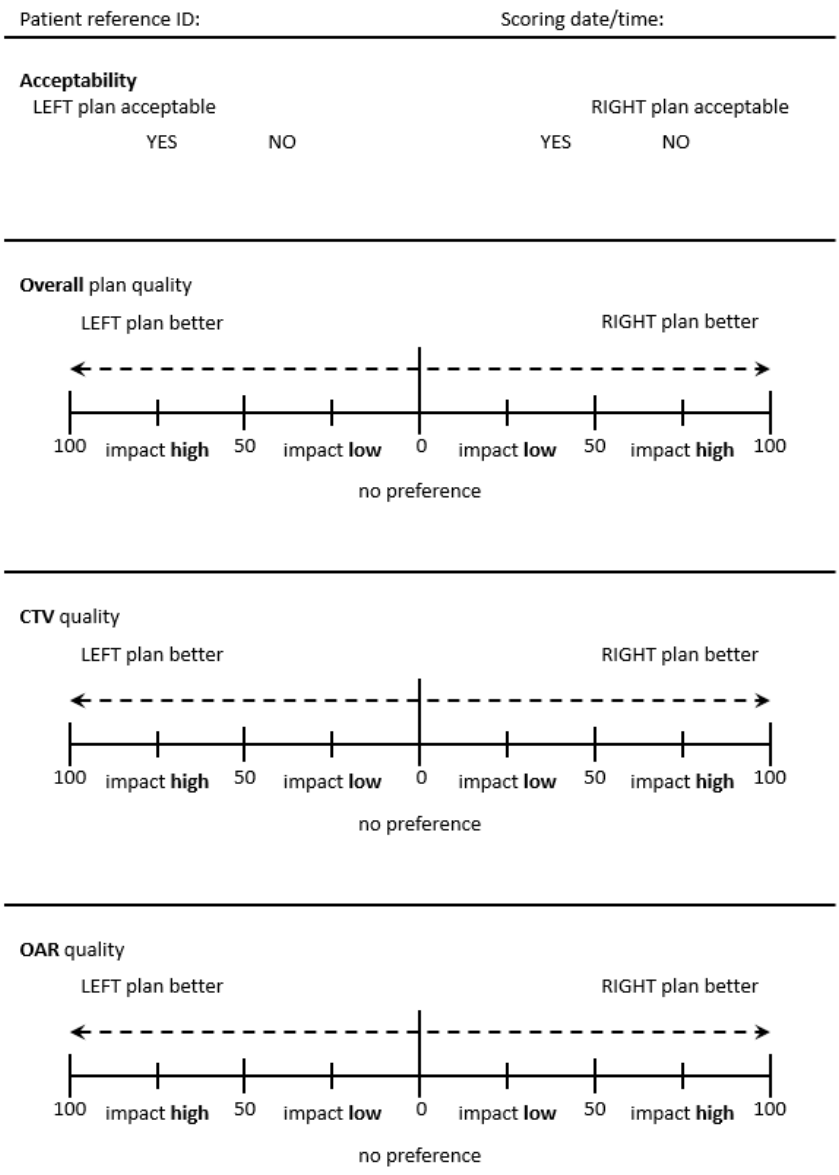

Figure 26: Scoring form in the blind comparison of PLAN_{auto} and PLAN_{ref}, provided to the expert clinician. The clinician first determined the clinical acceptability of the left and right plan, whereafter the plan quality was assessed in terms of *overall, CTV* and *OAR* quality using the visual analog scale.

Appendix E2 - Information sheet provided to clinican

Patiënt 29

1. **Patiënt informatie**
   Totaal aantal fracties: 3
   EBRT Dosis: 46 Gy
   Fractie nummer: 3
   Aantal naalden: 4

2. **DVH's**

Links

ROI	Dose [%]	Dose [cGy]	Volume [%]	Volume [...
Bladder	92.67	648.70	0.86	**2.00**
Bladder	102.86	**720.00**	0.37	0.85
GTV	**100.00**	700.00	100.06	1.21
GTV	234.52	1641.62	**90.00**	1.09
HR-CTV	**100.00**	700.00	99.45	28.64
HR-CTV	132.66	928.62	**90.00**	25.92
Rectum	45.23	316.62	2.26	**2.00**
Rectum	80.00	**560.00**	-	-
Sigmoid	81.01	567.07	2.74	**2.00**
Sigmoid	80.00	**560.00**	2.95	2.16
SmallBowel	31.77	222.39	6.17	**2.00**
SmallBowel	52.86	**370.00**	0.02	0.01

Rechts

ROI	Dose [%]	Dose [cGy]	Volume [%]	Volume [...
Bladder	92.71	648.94	0.86	**2.00**
Bladder	102.86	**720.00**	0.24	0.56
GTV	**100.00**	700.00	100.06	1.21
GTV	180.23	1261.63	**90.00**	1.09
HR-CTV	**100.00**	700.00	99.28	28.59
HR-CTV	119.66	837.63	**90.00**	25.92
Rectum	46.63	326.38	2.26	**2.00**
Rectum	80.00	**560.00**	-	-
Sigmoid	81.71	571.98	2.74	**2.00**
Sigmoid	80.00	**560.00**	3.17	2.32
SmallBowel	33.80	236.62	6.17	**2.00**
SmallBowel	52.86	**370.00**	0.03	0.01

3. **Informatie deze fractie**

	Links	Rechts
Bijdrage naalden	16%	8%
Bijdrage ovoiden	49%	54%
Bijdrage intra	35%	38%

4. **Informatie voorgaande fracties**

(Gy)	D90 HRCTV	D2cc Blaas	D2cc Rectum	D2cc Sigmoid	D2cc Dunne Darm
Fractie 1	7.5	7.7	2.8	5.5	3.3
Fractie 2	8.4	7.2	3.7	5.7	2.0

Figure 27: Example of an information sheet provided to the clinician in the blind comparison of PLAN_{auto} and PLAN_{ref}, in which the following information was provided: 1. Information about the patient: the total number of BT fractions, the dose received during EBRT, the current fraction number and the number of needles that were implanted in the current fraction. 2. Dosimetric measures from the DVHs computed in Oncentra Brachy for both the left and right plan. 3. The relative dosimetric contribution from the needles, ovoids and intra cavitairy channel of the applicator. 4. Dosimetric measures from previous clinical BT fractions.

References

[1] Tobias Achterberg. *Constraint Integer Programming*. PhD thesis, TU Berlin, 2007.

[2] Ron Alterovitz, Etienne Lessard, Jean Pouliot, I-Chow Joe Hsu, James F O'Brien, and Ken Goldberg. Optimization of HDR brachytherapy dose distributions using linear programming with penalty costs. *Medical physics*, 33(11):4012–4019, 2006.

[3] G Ayotte, M D'Amours, S Aubin, E Lessard, J Pouliot, and L Beaulieu. Sci—Thurs AM: YIS—02: Optimizing number and position of catheters within inverse planning simulated annealing (IPSA) for prostate and breast high dose rate brachytherapy. *Medical Physics*, 36(9Part3):4315–4315, 2009.

[4] D Baltas, Z Katsilieri, V Kefala, S Papaioannou, A Karabis, P Mavroidis, and N Zamboglou. Influence of modulation restriction in inverse optimization with HIPO of prostate implants on plan quality: Analysis using dosimetric and radiobiological indices. In *World Congress on Medical Physics and Biomedical Engineering, September 7-12, 2009, Munich, Germany*, pages 283–286. Springer, 2009.

[5] Jeroen Beliën, Jan Colpaert, Liesje De Boeck, and Erik Demeulemeester. A hybrid simulated annealing linear programming approach for treatment planning in HDR brachytherapy with dose volume constraints. In *Proc. of the 35th Int. Conf. on Operational Research Applied to Health Services*, 2009.

[6] Amit Ben Antony Bennan. Automated Treatment Planning in HDR brachytherapy for Prostate Cancer. Master's thesis, TU Delft, 2017.

[7] Sebastiaan Breedveld, Amit Bennan, Shafak Aluwini, Dennis Schaart, Kolkman Deurloo, and Ben Heijmen. Fast automated multi-criteria planning for HDR brachytherapy explored for prostate cancer. Submitted.

[8] Sebastiaan Breedveld, Pascal RM Storchi, Peter WJ Voet, and Ben JM Heijmen. iCycle: Integrated, multicriterial beam angle, and profile optimization for generation of coplanar and non-coplanar IMRT plans. *Medical physics*, 39(2):951–963, 2012.

[9] Sebastiaan Breedveld, Bas van den Berg, and Ben Heijmen. An interior-point implementation developed and tuned for radiation therapy treatment planning. *Computational Optimization and Applications*, 68(2):209–242, 2017.

[10] Enrique Chajon, Isabelle Dumas, Mahmoud Touleimat, Nicolas Magné, Jérémy Coulot, Rodolfe Verstraet, Dimitri Lefkopoulos, and Christine Haie-Meder. Inverse planning approach for 3-D MRI-based pulse-dose rate intracavitary brachytherapy in cervix cancer. *International Journal of Radiation Oncology* Biology* Physics*, 69(3):955–961, 2007.

[11] Timo M Deist and Bram L Gorissen. High-dose-rate prostate brachytherapy inverse planning on dose-volume criteria by simulated annealing. *Physics in Medicine & Biology*, 61(3):1155, 2016.

[12] Libni Eapen, Cathy Kayser, Yves Deshaies, Gad Perry, E Choan, Christopher Morash, Joanna E Cygler, David Wilkins, and Simone Dahrouge. Correlating the degree of needle trauma during prostate brachytherapy and the development of acute urinary toxicity. *International Journal of Radiation Oncology* Biology* Physics*, 59(5):1392–1394, 2004.

[13] Jacques Ferlay, Isabelle Soerjomataram, Rajesh Dikshit, Sultan Eser, Colin Mathers, Marise Rebelo, Donald Maxwell Parkin, David Forman, and Freddie Bray. Cancer incidence and mortality worldwide: sources, methods and major patterns in GLOBOCAN 2012. *International journal of cancer*, 136(5):E359–E386, 2015.

[14] D Giantsoudi, D Baltas, A Karabis, P. Mavroidis, N Zamboglou, N Tselis, C Shi, and N Papanikolaou. A gEUD-based inverse planning technique for HDR prostate brachytherapy: Feasibility study. *Medical physics*, 40(4), 2013.

[15] Bram L Gorissen, Dick Den Hertog, and Aswin L Hoffmann. Mixed integer programming improves comprehensibility and plan quality in inverse optimization of prostate HDR brachytherapy. *Physics in Medicine & Biology*, 58(4):1041, 2013.

[16] Christian V Guthier, Antonio L Damato, Juergen W Hesser, Akila N Viswanathan, and Robert A Cormack. A fast inverse treatment planning strategy facilitating optimized catheter selection in image-guided high-dose-rate interstitial gynecologic brachytherapy. *Medical physics*, 44(12):6117–6127, 2017.

[17] Christian V Guthier, Antonio L Damato, Akila N Viswanathan, Juergen W Hesser, and Robert A Cormack. A fast multitarget inverse treatment planning strategy optimizing dosimetric measures for high-dose-rate (HDR) brachytherapy. *Medical physics*, 44(9):4452–4462, 2017.

[18] CV Guthier, KP Aschenbrenner, R Müller, L Polster, RA Cormack, and JW Hesser. Real-time inverse high-dose-rate brachytherapy planning with catheter optimization by compressed sensing-inspired optimization strategies. *Physics in medicine and biology*, 61(16):5956–5972, 2016.

[19] Matthew M Harkenrider, Fiori Alite, Scott R Silva, and William Small Jr. Image-based brachytherapy for the treatment of cervical cancer. *International Journal of Radiation Oncology* Biology* Physics*, 92(4):921–934, 2015.

[20] Rens van Haveren, Ben JM Heijmen, and Sebastiaan Breedveld. Automatically configuring the reference point method for automated multi-objective treatment planning. *Physics in medicine and biology*, 2018.

[21] Ben Heijmen. Radiobiology and Bio-Physical models (photon and electron beams). University Lecture, 2018.

[22] Åsa Holm. A Tailored Branch-and-Bound Method for Optimizing the Dwelling Time Pattern and Catheter Positioning in HDR Brachytherapy. *Retrieved from http://urn.kb.se/resolve?urn=urn:nbn:se:liu:diva-99784*.

[23] Åsa Holm. *Mathematical optimization of HDR brachytherapy*. PhD thesis, Linköping University Electronic Press, 2013.

[24] Åsa Holm, Torbjörn Larsson, and Åsa Carlsson Tedgren. Impact of using linear optimization models in dose planning for HDR brachytherapy. *Medical physics*, 39(2):1021–1028, 2012.

[25] Åsa Holm, Torbjörn Larsson, and Åsa Carlsson Tedgren. A linear programming model for optimizing HDR brachytherapy dose distributions with respect to mean dose in the DVH-tail. *Medical physics*, 40(8):081705, 2013.

[26] Åsa Holm, Åsa Carlsson Tedgren, and Torbjörn Larsson. Heuristics for integrated optimization of catheter positioning and dwell time distribution in prostate HDR brachytherapy. *Annals of Operations Research*, 236(2):319–339, 2016.

[27] Xun Jia, Chunhua Men, Yifei Lou, and Steve B Jiang. Beam orientation optimization for intensity modulated radiation therapy using adaptive l2,1-minimization. *Physics in Medicine & Biology*, 56(19):6205, 2011.

[28] A Karabis, P Belotti, and D Baltas. Optimization of catheter position and dwell time in prostate HDR brachytherapy using HIPO and linear programming. In *World Congress on Medical Physics and Biomedical Engineering, September 7-12, 2009, Munich, Germany*, pages 612–615. Springer, 2009.

[29] Inger-Karine Kolkman-Deurloo. Brachytherapy, Medical Physics of Photon and Proton Therapy. University Lecture, 2018.

[30] M Lahanas, D Baltas, S Giannouli, N Milickovic, and N Zamboglou. Generation of uniformly distributed dose points for anatomy-based three-dimensional dose optimization methods in brachytherapy. *Medical physics*, 27(5):1034–1046, 2000.

[31] M Lahanas, D Baltas, and N Zamboglou. A hybrid evolutionary algorithm for multi-objective anatomy-based dose optimization in high-dose-rate brachytherapy. *Physics in Medicine & Biology*, 48(3):399, 2003.

[32] Etienne Lessard, I-Chow Hsu, and Jean Pouliot. Inverse planning for interstitial gynecologic template brachytherapy: truly anatomy-based planning. *International Journal of Radiation Oncology* Biology* Physics*, 54(4):1243–1251, 2002.

[33] B Morén, T Larsson, and Å Carlsson Tedgren. Mathematical optimization of high dose-rate brachytherapy—derivation of a linear penalty model from a dose-volume model. *Physics in Medicine & Biology*, 63(6):065011, 2018.

[34] Richard Pötter, Christine Haie-Meder, Erik Van Limbergen, Isabelle Barillot, Marisol De Brabandere, Johannes Dimopoulos, Isabelle Dumas, Beth Erickson, Stefan Lang, An Nulens, et al. Recommendations from gynaecological (GYN) GEC ESTRO working group (II): concepts and terms in 3D image-based treatment planning in cervix cancer brachytherapy—3D dose volume parameters and aspects of 3D image-based anatomy, radiation physics, radiobiology. *Radiotherapy and Oncology*, 78(1):67–77, 2006.

[35] Eric Poulin, Charles-Antoine Collins Fekete, Mélanie Létourneau, Aaron Fenster, Jean Pouliot, and Luc Beaulieu. Adaptation of the CVT algorithm for catheter optimization in high dose rate brachytherapy. *Medical physics*, 40(11), 2013.

[36] Eric Poulin, Emmanuel Racine, Dirk Binnekamp, and Luc Beaulieu. Fast, automatic, and accurate catheter reconstruction in HDR brachytherapy using an electromagnetic 3D tracking system. *Medical physics*, 42(3):1227–1232, 2015.

[37] Mark J Rivard, Bert M Coursey, Larry A DeWerd, William F Hanson, M Saiful Huq, Geoffrey S Ibbott, Michael G Mitch, Ravinder Nath, and Jeffrey F Williamson. Update of AAPM Task Group No. 43 Report: A revised AAPM protocol for brachytherapy dose calculations. *Medical physics*, 31(3):633–674, 2004.

[38] Mark J Rivard, Jack LM Venselaar, and Luc Beaulieu. The evolution of brachytherapy treatment planning. *Medical physics*, 36(6Part1):2136–2153, 2009.

[39] Linda Rossi, Sebastiaan Breedveld, Ben JM Heijmen, Peter WJ Voet, Nico Lanconelli, and Shafak Aluwini. On the beam direction search space in computerized non-coplanar beam angle optimization for IMRT—prostate SBRT. *Physics in Medicine & Biology*, 57(17):5441, 2012.

[40] Henri Ruotsalainen, Kaisa Miettinen, and Jan-Erik Palmgren. Interactive multiobjective optimization for 3D HDR brachytherapy applying IND-NIMBUS. In *New Developments in Multiple Objective and Goal Programming*, pages 117–131. Springer, 2010.

[41] Abdul Wahab M Sharfo, Peter WJ Voet, Sebastiaan Breedveld, Jan Willem M Mens, Mischa S Hoogeman, and Ben JM Heijmen. Comparison of VMAT and IMRT strategies for cervical cancer patients using automated planning. *Radiotherapy and Oncology*, 114(3):395–401, 2015.

[42] Chenyang Shen, Yesenia Gonzalez, Peter Klages, Nan Qin, Hyunuk Jung, Liyuan Chen, Dan Nguyen, Steve B Jiang, and Xun Jia. Intelligent Inverse Treatment Planning via Deep Reinforcement Learning, a Proof-of-Principle Study in High Dose-rate Brachytherapy for Cervical Cancer. *arXiv preprint arXiv:1811.10102*, 2019.

[43] Timmy Siauw, Adam Cunha, Alper Atamtürk, I-Chow Hsu, Jean Pouliot, and Ken Goldberg. IPIP: A new approach to inverse planning for HDR brachytherapy by directly optimizing dosimetric indices. *Medical Physics*, 38(7):4045–4051, 2011.

[44] Timmy Siauw, Adam Cunha, Dmitry Berenson, Alper Atamtürk, I-Chow Hsu, Ken Goldberg, and Jean Pouliot. NPIP: A skew line needle configuration optimization system for HDR brachytherapy. *Medical physics*, 39(7Part1):4339–4346, 2012.

[45] Kari Tanderup, Richard Pötter, Jacob Lindegaard, Christian Kirisits, Ina Juergenliemk-Schulz, Astrid de Leeuw, Israël Fortin, Kathrin Kirchheiner, Dietmar Georg, Remi Nout, Yvette Seppenwoolde, Wolfgang Dörr, Thomas Liederer, and Li Tee Tan. Image guided intensity modulated External beam radiochemotherapy and MRI based adaptive BRAchytherapy in locally advanced CErvical cancer. *retrieved from: https://www.embracestudy.dk/UserUpload/PublicDocuments/EMBRACE%20II%20Protocol.pdf.*

[46] Boon-Keng Teo, Lara P Bonner Millar, Xuanfeng Ding, and Lilie L Lin. Assessment of cumulative external beam and intracavitary brachytherapy organ doses in gynecologic cancers using deformable dose summation. *Radiotherapy and Oncology*, 115(2):195–202, 2015.

[47] Akila N Viswanathan, Sushil Beriwal, F Jennifer, D Jeffrey Demanes, David Gaffney, Jorgen Hansen, Ellen Jones, Christian Kirisits, Bruce Thomadsen, and Beth Erickson. American Brachytherapy Society consensus guidelines for locally advanced carcinoma of the cervix. Part II: high-dose-rate brachytherapy. *Brachytherapy*, 11(1):47–52, 2012.

[48] Akila N Viswanathan, Jennifer Moughan, William Small Jr, Charles Levenback, Revathy Iyer, Sharon Hymes, Adam P Dicker, Brigitte Miller, Beth Erickson, and David K Gaffney. The quality of cervical cancer brachytherapy implantation and the impact on local recurrence and disease-free survival in RTOG Prospective Trials 0116 and 0128. *International journal of gynecological cancer: official journal of the International Gynecological Cancer Society*, 22(1):123, 2012.

[49] Akila N Viswanathan, Bruce Thomadsen, American Brachytherapy Society Cervical Cancer Recommendations Committee, et al. American Brachytherapy Society consensus guidelines for locally advanced carcinoma of the cervix. Part I: general principles. *Brachytherapy*, 11(1):33–46, 2012.

[50] Peter WJ Voet, Sebastiaan Breedveld, Maarten LP Dirkx, Peter C Levendag, and Ben JM Heijmen. Integrated multicriterial optimization of beam angles and intensity profiles for coplanar and noncoplanar head and neck IMRT and implications for VMAT. *Medical physics*, 39(8):4858–4865, 2012.